İSTANBUL TECHNICAL UNIVERSITY ★ INSTITUTE OF SCIENCE AND TECHNOLOGY

SIMULATION AND ANALYSIS OF THREE-DIMENSIONAL SEPARATED FLOW AROUND BLUFF BODIES

M.Sc. Thesis by

Kürşat KARA

Department : Aeronautical Engineering

Programme: Aeronautical Engineering

MAY 2003

İSTANBUL TECHNICAL UNIVERSITY ★ INSTITUTE OF SCIENCE AND TECHNOLOGY

SIMULATION AND ANALYSIS OF THREE-DIMENSIONAL SEPARATED FLOW AROUND BLUFF BODIES

M.Sc. Thesis by
Kürşat KARA
(511991046)

Date of submission: 09 May 2003

Date of defence examination: 29 May 2003

Supervisor (Chairman): Prof. Dr. M. Fevzi ÜNAL

Members of the Examining Committee: Doç. Dr. Metin Orhan KAYA

Doç. Dr. Aydın MISIRLIOĞLU

MAY 2003

İSTANBUL TEKNİK ÜNİVERSİTESİ ★ FEN BİLİMLERİ ENSTİTÜSÜ

KÜT CİSİMLER ETRAFINDAKİ ÜÇ BOYUTLU AYRILMALI AKIŞIN BENZETİMİ VE ANALİZİ

YÜKSEK LİSANS TEZİ
Kürşat KARA
(511991046)

Tezin Enstitüye Verildiği Tarih : 09 Mayıs 2003
Tezin Savunulduğu Tarih : 29 Mayıs 2002

Tez Danışmanı : Prof. Dr. M. Fevzi ÜNAL
Diğer Jüri Üyeleri : Doç. Dr. Metin Orhan KAYA
Doç. Dr. Aydın MISIRLIOĞLU

MAYIS 2003

ACKNOWLEDGEMENTS

I would like to thank to my supervisor Prof. Dr. M. Fevzi ÜNAL for allowing me to study together on this exciting subject. I gratefully acknowledge his support.

I also appreciate valuable help of Dr. H. İbrahim KESER throughout my studies.

Finally, I would like to thank to my family. They have done everything for me. They have supported me to come here. I will never forget their support.

May, 2003 Kürşat KARA

CONTENTS

LIST OF FIGURES	**iv**
LIST OF SYMBOLS	**vi**
SUMMARY	**vii**
ÖZET	**viii**
1. INTRODUCTION	**1**
1.1. Historical Background	1
2. MATHEMATICAL MODEL	**5**
2.1. Governing Equations	6
2.2 Generalized Biot-Savart Law	8
2.3 Basis of Grid-Free Lagrangian Simulation	11
2.4 Vorticity Layer Spreading from the Solid Surface	13
2.5 Discrete Vortex Model	15
2.6 Diffusion Model of Vortex Blob	19
2.7 Panel Method	23
2.8 Calculation Procedure	25
3. RESULTS AND CONCLUSION	**26**
3.1 Flow Simulation around a Sphere (Re=1000)	26
3.2 Flow Simulation around a Circular Cylinder	32
3.2.1 Run Parameters for the Circular Cylinder	33
3.2.2 Case 1 (Simulation at Re=50)	34
3.2.3 Case 2 (Simulation at Re=200)	40
3.2.4 Case 3 (Simulation at Re=500)	48
3.3 Conclusions	51
REFERENCES	**53**
APPENDIX A1	**57**
BIOGRAPHY	**59**

LIST OF FIGURES

		Page No
Figure 2.1	: Flow field involving vorticity region……..	10
Figure 2.2	: Vorticity Layer Spreading Method…..……...	14
Figure 2.3	: Radially symmetric smoothing function $p_{(\rho)}$ ……..	19
Figure 2.4	: A radially symmetric vortex blob and its corresponding circular cylindrical stick……..……...	20
Figure 2.5	: Stretching of vortex blob and its corresponding circular cylindrical stick...……	21
Figure 2.6	: Diffusion of vortex blob and its corresponding circular cylindrical stick...……	21
Figure 2.7	: New vortex blob after stretching and diffusion……...	21
Figure 3.1	: Panel configuration of sphere.…….	26
Figure 3.2	: Flow pattern around sphere (T=2.0)……	26
Figure 3.3	: Flow pattern around sphere (T=9.0)……..…..	26
Figure 3.4	: Side view of discrete vortex flow pattern around sphere at the elapsed times T=0, 1.0, 2.0, 3.0, 4.0, 5.0, 6.0, 7.0, 8.0, and 9.0 (Re=1000)…….……..	27
Figure 3.5	: 3D discrete vortex flow patterns around sphere at the elapsed times T=0, 1.0, 2.0, 3.0, 4.0, 5.0, 6.0, 7.0, 8.0, and 9.0 (Re=1000)……..	29
Figure 3.6	: Views of circular cylinder and sidewalls……	30
Figure 3.7	: Calculated body, images of the body and side walls……..	31
Figure 3.8	: Perspective view of circular cylinder……..	31
Figure 3.9	: Wake structures of circular cylinder in xy plane from T=0.0 to T=11.0. Re=50……..	33
Figure 3.10	: Wake structures of circular cylinder in xz plane from T=0.0 to T=11.0. Re=50……..	35
Figure 3.11	: Perspective view of wake structures of circular cylinder from T=0.0 to T=11.0. Re=50…….	37
Figure 3.12	: Wake structures of circular cylinder in xy plane from T=0.0 to T=7.0. Re=200…….....	39
Figure 3.13	: Wake structures of circular cylinder in xy plane from T=8.0 to T=15.0. Re=200…….....	40
Figure 3.14	: Wake structures of circular cylinder in xy plane from T=16.0 to T=21.0. Re=200……..…….....	41
Figure 3.15	: Wake structures of circular cylinder in xz plane from T=0.0 to T=7.0. Re=200…….....	42
Figure 3.16	: Wake structures of circular cylinder in xz plane from T=8.0 to T=20.0. Re=200…….....	43

Figure 3.17 : Perspective view of wake structures of circular cylinder from T=0.0 to T=7.0. Re=200……..…… 44
Figure 3.18 : Perspective view of wake structures of circular cylinder from T=8.0 to T=15.0. Re=200……..……..…… 45
Figure 3.19 : Perspective view of wake structures of circular cylinder from T=16.0 to T=21.0. Re=200…….…… 46
Figure 3.20 : Wake structures of circular cylinder in XY plane, from T=0.0 to T=6.0. Re= 500...…….. 48
Figure 3.21 : Wake structures of circular cylinder in XZ plane, from T=0.0 to T=6.0. Re=500...……...… 49
Figure 3.22 : Perspective view of wake structure of circular cylinder from T=0.0 to T=6.0. R= 500…… 50

LIST OF SYMBOLS

$\mathbf{D}$	: Cylinder diameter
$\mathbf{T}$	: Dimensionless time ($t\ U_\infty /D$)
$\mathbf{U_\infty}$	: Free Stream Velocity
$\mathbf{\Delta t}$	: Time step of calculation
$\vec{\mathbf{U}}$	: Velocity vector
$\mathbf{t}$	: Time
$\mathbf{p}$	: Pressure
ρ	: Density
υ	: Kinematic viscosity
ω	: Vorticity
$\mathbf{A}$	: Potential function
$\mathbf{S_{1,2}}$	: Boundary surfaces
$\mathbf{G}$	: Fundamental solution of the scalar Laplace equation
$\mathbf{Re}$	: Reynolds number based on D
$\mathbf{R}$	: Position vector
σ	: Source strength
γ	: Vortex strength
Γ	: Circulation
$\mathbf{V}$	: Volume
ε_i	: Core radius of $i.^{th}$ vorton
α_i	: Vortex strength
ω_{0i}	: Vortex distribution function
$\mathbf{u_i}$	: Induced velocity of $i.^{th}$ vorton
$\mathbf{P_{(\rho)}}$	: Radially symmetric smoothing function
$\mathbf{[K]}$	: Geometry matrix
$\mathbf{[RHS]}$	: Right hand side vector
$\mathbf{[\sigma]}$	: Source strength vector

SIMULATION AND ANALYSIS OF THREE-DIMENSIONAL SEPERATED FLOW AROUND BLUFF BODIES

SUMMARY

Owing to its importance in many engineering applications, including heat exchangers, risers in marine technology, road vehicles, building and bridges, flow around bluff bodies has been subject to numerous experimental and computational studies.

In contrast to the view expressed in many computational studies of flow around bluff bodies, even the fundamental flow case of a nominally two-dimensional body, e.g. a circular cylinder in a uniform stream exhibits several three-dimensional features. Strictly, two-dimensional geometries and two-dimensional flows can only exist in theoretical models, since in reality, all bodies have finite lateral extents and, above some critical Reynolds number, all flows generate instabilities with some spanwise wavelength.

Consequently, in recent years increasing experimental and numerical research effort is being directed towards three-dimensional features of nominally two dimensional, mildly or strongly three-dimensional bluff bodies.

In this study, using a three-dimensional discrete vortex method, separated flow around bluff bodies has been simulated. Simulation is based on the panel method for surface representation of body surfaces and tracing of panels released into the flow field from body surface for separated flow simulation. The simulation method is fully Lagrangian and thus does not require a grid around the bodies. A sphere and a circular cylinder are investigated at various Re numbers. Computations have been carried out using Fortran compiler on a High Performance Computation System available at ITU. The computer code has been developed to be applicable not only to the case of circular cylinder but also to the flow around arbitrary, complex geometries.

KÜT CİSİMLER ETRAFINDAKİ ÜÇ BOYUTLU AYRILMALI AKIŞIN BENZETİMİ VE ANALİZİ

ÖZET

Isı değiştiriciler, açık deniz platformları, kara taşıtları, binalar ve köprüler gibi farklı mühendislik uygulamalarındaki önemi nedeniyle küt cisimler etrafındaki akış alanı birçok deneysel ve sayısal çalışmaya konu olmuştur.

Sayısal çalışmaların çoğunluğunda göz önüne alınanın aksine iki boyutlu olarak adlandırılan cisimler etrafındaki temel akış hali, örneğin uniform akış alanı içindeki dairesel silindir bile çeşitli üç boyutlu özellikler göstermektedir. Gerçekte, bütün cisimler sonlu bir genişliğe sahip olduğu için, belirli bir kritik Reynolds sayısından sonra bütün akışlar genişlik boyunca belirli bir dalga boyuyla kararsızlık geliştirmekte ve dolayısıyla iki boyutlu geometriler ve iki boyutlu akışlar sadece teorik olarak mümkün olabilmektedir.

Dolayısıyla, son yıllarda deneysel ve sayısal çalışmalarda dikkatler artan bir oranda iki boyutlu olarak adlandırılan, hafifçe üç boyutluluğa sahip olan veya kuvvetli bir üç boyutluluk gösteren geometriler etrafındaki akışlara çevrilmiştir.

Bu çalışmada, üç boyutlu Ayrık Vorteks Yöntemi kullanılarak küt cisimler etrafındaki üç boyutlu ayrılmalı akış simule edilmiştir. Simulasyon yöntemi cisim yüzeylerinin paneller ile temsiline ve ayrılmalı akışın hesaplanması için cisim yüzeyinden belirli zaman aralıkları ile akım alanı içine bırakılan vorteks panellerin hareketleri boyunca izlenmesi esasına dayanmaktadır. Tamamen Lagrange'sal olan bu yöntemde küt cisimler etrafında bir çözüm ağı üretmek gerekli değildir. Küre ve dairesel silindir etrafındaki akış yapıları çeşitli Re sayılarında incelenmiştir. Hesaplamalar, İTÜ'de var olan Yüksek Başarımlı Hesaplama Sistemleri kullanılarak paralel hesaplama ile yapılmıştır. Bilgisayar kodu karmaşık cisimler etrafındaki akışa da uygulanabilir olacak şekilde geliştirilmiştir.

1. INTRODUCTION

1.1 Historical Background

Flow around bluff bodies has long been of fundamental interest. References to flow separation from bluff bodies date back to as early as the ancient times. It was then described that a tensioned wire placed in a wind flow produces sound, which is called the “Aeolian Tones” [1].

In the past thirty years, the vortex methods have been developed and applied for analysis of complex vortical flow and simulation of unsteady flow related with problems in various engineering fields, since they are standing on simple algorithm based on physics of flow, and their numerical stability is usually quite well [2]. Recently, not only from the increasing requirements for numerical simulation of much more complicated unsteady flows in engineering fields, but also from physical interests in investigation of fine scale vortex structures in viscous unsteady flows, many basic studies have been carried out to extend the applicability of the vortex methods and to improve the reliability on their calculation results. Leonard [3] summarized the basic algorithm and examples of its application to fundamental flows, and Sarpkaya [1] presented a comprehensive review of various vortex methods, making use of Lagrangian or mixed Lagrangian-Eulerian schemes, or the direct Biot-Savart law and the Vortex in Cell methods respectively. It is known that in the Lagrangian method, one does not need to generate grids for estimation of velocities in the flow field, and so the method has been applied to flows of high Reynolds numbers. On the other hand, the grid generation is necessary in the Vortex in Cell method, which has been applied to flows of rather low Reynolds numbers.

One of the most important points in the recent vortex methods is how to threat viscous diffusion in the computation procedure. Graham developed the Vortex in Cell method incorporating viscous diffusion in which convection of vorticity is modeled by

Lagrangian scheme and diffusion by an Eulerian scheme [4], and Meneghini and Bearman [5] applied the method to simulate the flow about an oscillating circular cylinder at a low Reynolds number (Re = 200). As regard with the expression of viscous diffusion of vorticity in the Lagrangian methods, various schemes like the core spreading method by Kuwahara and Takami, the random walk method by Chorin and the integrated vorticity equation method by Winkelmans and Leonard have been proposed as referred to in [3]. The feature of core spreading method was discussed by Leonard [3] and it was applied to the three dimensional analysis of the flow around a circular disk by Shriyama [6]. Although its convergence to the correct equation of motion was argued by Greengard, the core spreading method has been used extensively [7]. On the other hand, the random walk method was extended to the representation of vorticity diffusion in the proximity of a solid surface by Chorin and Lewis, who proposed the Random Vortex Method and Surface Vortex Method, respectively [2]. Furthermore, the random walk method was applied to represent the development of two-dimensional boundary layer making use of vortex sheets by Cheer who proposed Random Vortex Sheet Method [8]. Kida applied the method to investigate far-field condition of vortex methods on an impulsively started two-dimensional circular cylinder with rotation [2]. Recently, Nakanishi and Kamemoto [9] developed the Biot-Savart law method combined with the Panel Method and extended the Surface Vortex Method for the application to either two or three dimensional analysis of viscous flow, and Nakanishi [10] proposed a simple way to solve the pressure Poisson equation by a boundary integration technique for calculation of pressure distribution in the flow field computed by vortex methods. Their works summarized by Kamemoto who proposed the Vorticity Layer Spreading Method for expression of vorticity diffusion from solid surfaces [2].

In relation with various problems in engineering fields, the development of computer simulation methods has been expected for the prediction of unsteady flow characteristics around a stationary or an oscillating body. Despite the rapid developments of computational fluid dynamics, the numerical analysis of a higher Reynolds number flow around a moving boundary concerning with flow induced vibration problems still seems to be a difficult one, since the treatment of moving fine grids around the boundary is

usually complicated in computation by a finite difference or a finite element method. Moreover, the applicability of the conventional turbulence models of time-mean type seems to be questionable as far as the problems related with unsteady flow separation or flow induced vibration are concerned.

From the view point of engineering applications, it might be natural to consider that the simple algorithm and the stable properties of the vortex methods are remarkably attractive for the numerical investigation of unsteady vortical flows of higher Reynolds numbers. Among the various types of vortex methods developed in the past, the Lagrangian method combined with the Panel Method is considered to be one of the simplest methods, in which the boundary conditions of not only stationary but also moving bodies are easily introduced in a grid-free computation, and a complex configuration of boundary is easily represented by distributions of source and/or vortex panels [2].

On the other hand, the physics of the flow around bluff bodies is rather complicated. In contrast to the view expressed in many computational studies of flow around bluff bodies, even the fundamental flow case of a nominally two dimensional body, e.g. a circular cylinder in a uniform stream exhibits several three-dimensional features and at low Reynolds numbers, maintaining parallel vortex shedding to the cylinder axis requires very carefully controlled end conditions by means of suitably angled end plates or with other types of end constraint [11]. At high Reynolds numbers, two-dimensional shedding is possible only with a strong external influence such as body or flow oscillation in synchronization with shedding. Strictly, two-dimensional geometries and two-dimensional flows can only exist in theoretical models, since in reality, all bodies have finite lateral extents and, above some critical Reynolds number, all flows generate instabilities with some spanwise wavelength [12].

Consequently, in recent years increasing experimental and numerical research effort is being directed towards three-dimensional features of nominally two dimensional, mildly or strongly three-dimensional bluff bodies. Since key three-dimensional features of the wake of a nominally two-dimensional body, such as vortex dislocations, appear apparently randomly in time and space, Tombazis and Bearman [13] attempted to

control their locations by applying a mild geometric disturbance in the form of a wavy trailing edge. They made interesting observations about a number of distinct vortex shedding patterns. Several other authors have reported results of investigations that might also be described as mild [12]. More recently, Owen have shown that above a certain value of wave height to length ratio of the waviness the regular vortex shedding can no longer be detected behind a circular cylinder with a wavy axis and associated with this, sizeable reductions in drag can be achieved [12].

In the present study, a fully Lagrangian discrete vortex method is employed to simulate separated three-dimensional flow around circular cylinder and sphere. Surface representation of the bodies is performed by means of source and vortex panels distributed on the boundary surface. Strengths of the source and vortex panels are obtained by using the normal velocity condition at the surface of the cylinder and the conservation of vortex strength principle, respectively. As previously applied by Nakanishi and Kamemoto [9], the separated flow that is the vorticity field around bodies is represented by a number of vortex panels shed into the flow field from the surface. In order to reduce the computation time, after a prescribed distance from the surface, the panels in the flow field are converted into discrete vortices with spherically symmetric distribution of vorticity, i.e. vortons. The following chapter describes the mathematical basis and application details of the method.

2. MATHEMATICAL MODEL

In the vortex method, continuous distribution of vorticity is replaced with a number of vortex elements, and unsteady flow is analyzed by calculating motion and variation of vorticity of the vortex elements in Lagrangian manner. Therefore, it is rather easy to represent a high Reynolds number flow in which vortical flow fields exist in restricted regions.

The vortex models proposed previously can be categorized as a filament model, a stick model, a vorton model. The filament model is effective in simulating three-dimensional instability in two-dimensional shear layers [14]. However, it is known that the filament model leads to unrealistically strong vorticity when the filament is stretched in the direction of the vorticity axis. Therefore, it seems difficult to apply the filament model to complex rotational flows. However, the stick model can be used for calculation of the diffusion of vorticity in the vorton model. In the vorton model, it is known that trajectories of the vortex elements converge to those analyzed from the Euler equation as long as the smooth velocity field is retained in the calculation [15].

However, the calculated velocity field is not always smooth due to the lack of consideration of viscous diffusion. In order to consider the viscous effect, a random walk method and a method using an integral operator of the viscous term of the vorticity equation have been previously proposed [16]**.** However, from the viewpoint of engineering application, a simpler procedure for viscous effect consideration is expected. Nakanishi et al [15] proposed a simpler blob model for consideration of the viscous effect. They applied the model to the simulation of interaction between two vortex rings.

As mentioned previously, among the various types of vortex methods developed in the past, the Lagrangian method combined with the panel method is considered one of the simplest methods, in which the boundary conditions of not only stationary but also moving bodies [14] are easily introduced in the grid free computation, and a

complex configuration of boundary is easily represented by distributions of source and/or vortex panels [2].

In this study, attention is focused on the latter vortex method based on the Biot-Savart law as a convenient tool of numerical investigation of unsteady and vortical flow. In the following chapters the mathematical basis of the model is explained and flow structures obtained by the method for sphere and circular cylinder are presented.

2.1 Governing Equations

Since the vortex methods have been developed for numerical analysis of incompressible and unsteady flow, their governing equations are thought to be based on Navier-Stokes equation and the continuity equation for incompressible flow, which may be written in vector form as follows.

$$\frac{\partial \mathbf{u}}{\partial t} + (\mathbf{u} \cdot \nabla)\mathbf{u} = -\nabla\left(\frac{p}{\rho}\right) + \nu \nabla^2 \mathbf{u} \tag{2.1}$$

Replacing the nonlinear term by its equivalent form given by the identities in Appendix A, this vector equation becomes

$$\frac{\partial \mathbf{u}}{\partial t} + \nabla\left(\frac{1}{2}\mathbf{u} \cdot \mathbf{u}\right) - \mathbf{u} \times (\nabla \times \mathbf{u}) = -\nabla\left(\frac{p}{\rho}\right) + \nu \nabla^2 \mathbf{u} \tag{2.2}$$

The vorticity equation is obtained by taking the curl of this equation and noting that the curl of the gradient of any scalar is zero. Hence

$$\frac{\partial \mathbf{w}}{\partial t} - \nabla \times (\mathbf{u} \times \mathbf{w}) = \nu \nabla^2 \mathbf{w} \tag{2.3}$$

Using a vector identity given in Appendix A, the second term of the left hand side may be expanded to give

$$\nabla \times (\mathbf{u} \times \mathbf{w}) = \mathbf{u}(\nabla \cdot \mathbf{w}) - \mathbf{w}(\nabla \cdot \mathbf{u}) - (\mathbf{u} \cdot \nabla)\mathbf{w} + (\mathbf{w} \cdot \nabla)\mathbf{u} \tag{2.4}$$

But $\nabla \cdot \mathbf{w} = 0$, since the divergence of the curl of any vector is zero and $\nabla \cdot \mathbf{u} = 0$ from the continuity equation. Hence the vorticity equation becomes

$$\frac{\partial \mathbf{w}}{\partial t} + (\mathbf{u} \cdot \nabla)\mathbf{w} = (\mathbf{w} \cdot \nabla)\mathbf{u} + \nu \nabla^2 \mathbf{w} \tag{2.5}$$

For two-dimensional flows the vorticity vector w will be perpendicular to the plane of the flow, so that $(\mathbf{w}\cdot\nabla)\mathbf{u}$ will be zero. Then

$$\frac{\partial \mathbf{w}}{\partial t} - (\mathbf{u}\cdot\nabla)\mathbf{w} = \nu\nabla^2\mathbf{w} \tag{2.6}$$

where the vorticity **w** is defined as

$$\mathbf{w} = \nabla \times \mathbf{u} \tag{2.7}$$

Equations (2.5) and (2.7) are the governing equations of the vortex methods. As we can eliminate the vorticity **w** in (2.5) by substituting (2.7), it is easily understood that the velocity field represented by **u** can be calculated using (2.5) and (2.7), without necessity of solving pressure *p*. This fact is one of the most attractive features of the vortex methods.

On the other hand, if we take divergence of Navier Stokes equation(2.1), the pressure Poisson equation is derived.

$$\nabla^2 p = -\rho\nabla\cdot(\mathbf{u}\cdot\nabla\mathbf{u}) \tag{2.8}$$

Equation (2.8) shows that the pressure distribution *p* can be estimated directly from the instantaneous velocity field regardless of both unsteadiness and viscosity, as far as an incompressible flow is concerned. In the vortex methods, therefore, once the velocity field calculated, the pressure field can be obtained from (2.8) at any time if required.

2.2 Generalized Biot-Savart Law

Considering practical applications of the vortex methods, it seems that there exist a couple of important procedures. One of them is how to represent the vorticity distributions in a viscous and incompressible flow field. Another is how to represent the configuration of the flow boundary. In order to understand these matters, let us examine the generalized Biot-Savart law, because it forms the mathematical basis to the vortex method applied in this thesis.

If we introduce a function of a vector potential **A** to velocity vector *u* in a viscous and incompressible flow, it can be defined as

$$\mathbf{u} = \nabla \times \mathbf{A} \tag{2.9}$$

As it is generally known that the vector operation of $\nabla \cdot (\nabla \times \mathbf{A})$ is always equal to zero for any vector, divergence of (2.9) gives

$$\nabla \cdot \mathbf{u} = \nabla \cdot (\nabla \times \mathbf{A}) = 0 \tag{2.10}$$

Therefore, it is easily understood that the equation (2.9) satisfies the continuity equation for incompressible flow. If we substitute (2.9) for **u** in (2.7), we obtain another expression for the definition of vorticity using A as follows.

$$\mathbf{w} = \nabla \times \mathbf{u} = \nabla \times (\nabla \times \mathbf{A}) = \nabla (\nabla \cdot \mathbf{A}) - \nabla^2 \mathbf{A} \tag{2.11}$$

If we take account of the uniqueness of solution, the following solenoidal condition for A is introduced.

$$\nabla \cdot \mathbf{A} = 0 \tag{2.12}$$

Then, if we introduce (2.12) to (2.11), a vector Poisson equation is obtained as

$$\nabla^2 \mathbf{A} = -\mathbf{w} \tag{2.13}$$

As previously explained by Wu and Thompson as referred to in [2] in their study of integro -differential formulation of Navier Stokes equation, integration of the Poisson equation (2.13) with the aid of vector Green-formulae and Gaussian divergence theorem, provides the generalized Biot-Savart law represented by

$$\begin{aligned} u_{(r)} = & \int_V \omega_0 \times \nabla_0 G dV_0 - \\ & \int_{S_1+S_2} \left[(n_0 \cdot u_0) \nabla_0 G + (n_0 \times u_0) \times \nabla_0 G \right] dS_0 \end{aligned} \tag{2.14}$$

here, subscript [$_0$] denotes variable, differentiation and integration at a location r_0, and n_0 denotes the normal vector at a point on a boundary surface S_1 and S_2. And G is the fundamental solution of the scalar Laplace equation with a delta function δ in the right hand side as

$$\nabla^2 G = -\delta\left(r - r_0\right) \tag{2.15}$$

the solution of (2.15) are known as follows,

$$G = \frac{1}{2\pi}\ln\left(\frac{1}{\mathbf{R}}\right) \qquad [2D] \tag{2.16}$$

$$G = \frac{1}{4\pi\mathbf{R}} \qquad [3D] \tag{2.17}$$

here, $\mathbf{R} = r - r_0$, $R = |\mathbf{R}| = |r - r_0|$.

If we substitute (2.16) and (2.17) into (2.14), we obtain practical expression for the generalized Biot-Savart law,

$$\begin{aligned} u_{(r)} = & \frac{1}{\alpha}\int_V \frac{\omega_0 \times \mathbf{R}}{\mathbf{R}^\beta} dV_0 - \\ & \frac{1}{\alpha}\int_{S_1+S_2}\left[\frac{\left(n_0 \cdot u_0\right)\mathbf{R}}{\mathbf{R}^\beta} + \frac{\left(n_0 \times u_0\right)\times\mathbf{R}}{\mathbf{R}^\beta}\right] dS_0 \end{aligned} \tag{2.18}$$

here, $\alpha = 2\pi, \beta = 2$ for two-dimensional flow, and $\alpha = 4\pi, \beta = 3$ for three dimensional flow.

In (2.18), the inner product $n_0 \cdot u_0$ and the outer product $n_0 \times u_0$ stand for respectively normal and tangential velocity components on the boundary surface, and they respectively correspond to source and vortex distributions on the boundary surfaces. It follows that the equation (2.18) is considered to demonstrate how a velocity of viscous and incompressible flow is arrived at by the field integration of vorticity distributions and the surface integration of the source and vortex distributions. Writing the strengths of source and vortex on the boundary surfaces as σ_0 and γ_0 respectively, one can obtain an alternative expression to the generalized Biot-Savart law (2.18) as follows.

$$u_{(r)} = \frac{1}{\alpha}\int_{V}\frac{\omega_0 \times \mathbf{R}}{\mathbf{R}^{\beta}}dV_0 - \frac{1}{\alpha}\int_{S_1+S_2}\left[\frac{\sigma_0 \mathbf{R}}{\mathbf{R}^{\beta}} + \frac{\gamma_0 \times \mathbf{R}}{\mathbf{R}^{\beta}}\right]dS_0 \tag{2.19}$$

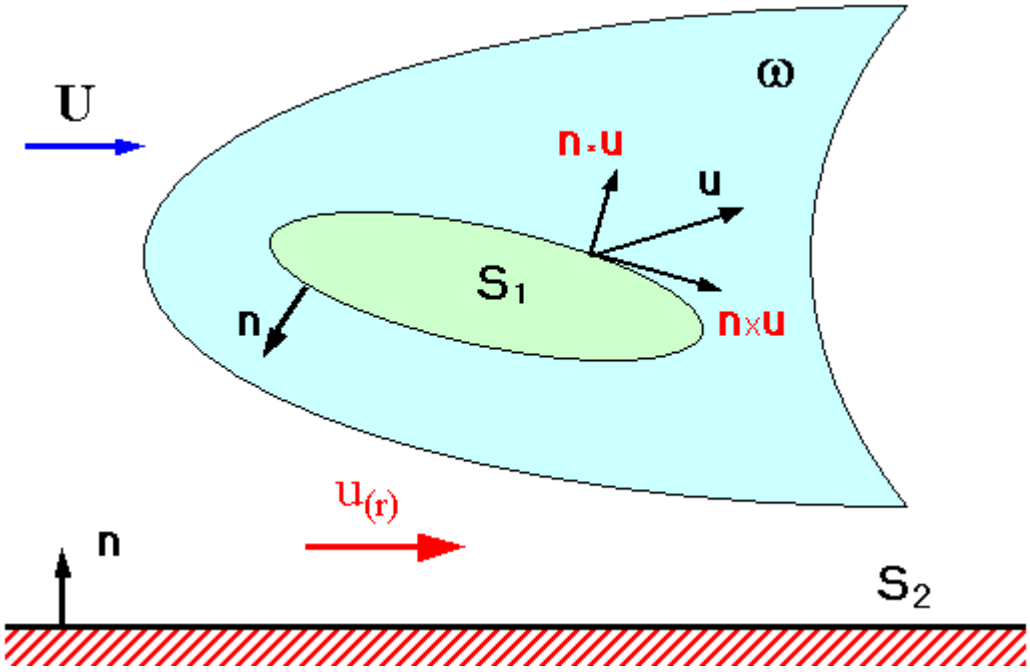


Figure 2.1: Flow field involving vorticity region.

Therefore, once the vorticity distributions are approximated by discrete vortices in the flow field, one can calculate the strengths of the source and/or vortex distributed along the boundary surfaces so as to satisfy the boundary conditions of normal and tangential velocity components on it, by numerically solving the integral equation. Then, the configuration of a flow boundary is easily represented by distributions of source and/or vortex panels around it, which are directly related with the velocity conditions on the boundary. Eventually, it is concluded that the present vortex method seems essentially suitable for the investigation of not only the flow around a complex configuration but also the unsteady flow around a moving boundary [14].

2.3 Basis of Grid-Free Lagrangian Simulation

As explained in the former section, the governing equations of the vortex methods are consisting of the vorticity transport equation(2.5), and the vorticity definition Equation (2.7), whereas the Biot-Savart law (2.18) is based on the latter equation. If we substitute the velocity **u** estimated from the Biot-Savart into (2.5), the unsteady transportation of vorticity is analyzed by solving the vorticity transport equation. As the Equation (2.5) is expressed in the Eulerian coordinates system, we can rewrite it using the expression for the material derivative $D/Dt = \partial/\partial t + (\mathbf{u}\cdot\nabla)$

$$\frac{D\mathbf{w}}{Dt} = \frac{\partial \mathbf{w}}{\partial t} + (\mathbf{u}\cdot\nabla)\mathbf{w} \tag{2.20}$$

Then, instead of (2.5), another expression of vorticity transport may be given in the Lagrangian form, which defines vorticity together with fluid particle as follows:

$$\frac{\partial \mathbf{w}}{\partial t} = (\mathbf{w}\cdot\nabla)\mathbf{u} + \nu\nabla^2\mathbf{w} \tag{2.21}$$

If we consider the vorticity of a fluid particle at a location r_0 at time t, the rate of variation of vorticity with time is represented by

$$\left(\frac{\partial \mathbf{w}}{\partial t}\right)_0 = (\mathbf{w}\cdot\nabla)_0\mathbf{u}_0 + \nu\left(\nabla^2\mathbf{w}\right)_0 \tag{2.22}$$

Therefore, writing the vorticity of the fluid particle at time t as $\omega_{0(t)}$, we obtain an approximate expression of the transportation of vorticity while the fluid particle moves during a small time interval dt as follows.

$$\omega_{0(t+dt)} = \omega_{0(t)} + \left(\omega\cdot\nabla\right)_0\mathbf{u}_0 dt + \nu\left(\nabla^2\omega\right)_0 dt \tag{2.23}$$

In (2.23), the second term on the right hand side is the three-dimensional convection of vorticity, which always becomes zero for two-dimensional flow, and the third term is the rate of viscous diffusion of vorticity. If the Reynolds number of the flow is sufficiently high, the convection term is considered much larger then the diffusion term, and thus, the third term in (2.23) may be neglected in the computation. Furthermore, if the high Reynolds number flow is two-dimensional, the equation (2.23) is approximated by the simple equation $\omega_{0(t+dt)} = \omega_{0(t)} = const.$ Therefore, if we take a small sectional area *ds* for the fluid particle and the vorticity is assumed

constant in this area, the two-dimensional fluid particle is thought a free vortex element which transports a constant circulation $\Gamma_0 = \omega_0 ds$

On the other hand, a Lagrangian form of a simple differential equation represents the motion of the fluid particle and the moving boundary.

$$\frac{dr_0}{dt} = u_0 \tag{2.24}$$

Then, the trajectory of the fluid particle over a time step dt is approximately computed from Euler method or the Adams-Bashforth method as follows.

$$r_{0(t+dt)} = r_{0(t)} + u_0 dt \tag{2.25}$$

$$r_{0(t+dt)} = r_{0(t)} + \left(1.5u_{0(t)} - 0.5u_{0(t-dt)}\right)dt \tag{2.26}$$

If the vorticity layers existing in the flow field are represented with discrete vortex distributions, the strengths of the source and/or vortex distributed along the boundary surface are numerically calculated in order to satisfy the boundary conditions of normal and tangential velocity components on it, by applying the popular scheme of the panel method to integral equation (2.19). Then, once the source and/or vortex distributions are determined on the right hand side of (2.19), not only a flow velocity at an arbitrary position in the flow field but also the convective velocity of each discrete vortex can be calculated. Substituting the velocities into (2.23) and (2.25) or (2.26), the vorticity transport and trajectory of each discrete vortex over the time step are numerically investigated, which provides new distribution of discrete vortices corresponding to the vorticity layers transported during the time step. Consequently, the iteration of the above procedure provides the basic scheme of grid-free Lagrangian simulation of unsteady, incompressible and viscous flow, making use of the Biot-Savart law vortex method.

2.4 Vorticity Layer Spreading From the Solid Surface

Vorticity generation and diffusion in the flow field near the solid surface is represented by reasonable distributions of discrete vortices so as to satisfy the no slip velocity condition on the solid surface. Then, the boundary layer development and separation are investigated from the calculation of convective and diffusive motion of the discrete vortices.

In order to take account of the vorticity diffusion from the solid surface, vortex sheet elements and/or source panels are distributed around the solid surface so that the normal and tangential velocity conditions of the boundary are satisfied on the surface. In the same manner as the viscous diffusion of vorticity in the shear layer over a suddenly accelerated flat plate explained by Schlichting [17] as the Stokes' first problem or the Rayleigh problem, the surface vorticity generated by the difference between the tangential velocity of the flow calculated on the solid surface and the tangential velocity of the solid wall itself, is considered to diffuse from the solid surface. Then, the nascent vorticity layer spreads from the solid surface to the flow field. In order to model this mechanism, nascent discrete vortices are introduced near the body surface in the Surface Vortex Method proposed by Kuwahara [18] and Lewis [19], and nascent vortex sheets of the surface vorticity are introduced in the Surface Vorticity Method proposed by Chorin [20] and Cheer [21]. However, the positions of the nascent vortices or vortex sheets in those methods are not determined physically, but assumed empirically. On the other hand, in the Vorticity Layer Spreading Method developed by Kamemoto [22], the nascent vortex sheets are introduced at a small distance δ_{dif} from the surface, as shown in Figure 2.2, where the distance δ_{dif} is given by the displacement thickness of the Stokes' first problem or Rayleigh problem which defines spreading of vorticity from the solid surface during a small time step *dt*. In the Rayleigh problem, is known [17] that when a flat plate is suddenly accelerated from rest and moves in its own plane (x direction) with a constant velocity U_0, the velocity distribution in the transverse section (y direction) over the surface is given as

$$u = U_0(1 - erf\,\eta) \tag{2.27}$$

here, $\eta = \frac{y}{2\sqrt{\nu t}}$, and $erf\,\eta = \frac{2}{\sqrt{\pi}}\int_0^{\eta} \exp(-\eta^2)d\eta$. Therefore, the displacement thickness δ_{dif} of the relative velocity distribution $(U_0 - u)$ during the elapsed time $t = dt$ is expressed as

$$\delta_{dif} = 1.136(\nu dt)^{1/2} \tag{2.28}$$

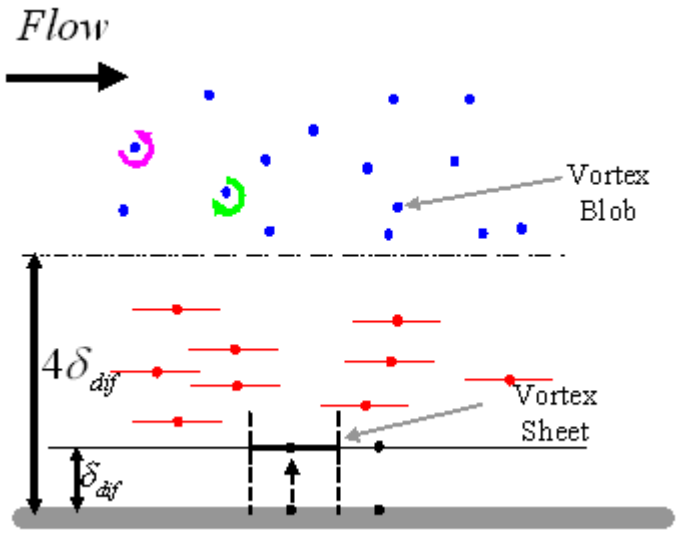


Figure 2.2: Vorticity Layer Spreading Method.

In this method, a nascent vortex sheet moves to a new position according to convective motion of its tangential velocity and further diffusion normal to the solid surface given by substituting the elapsed time in stead of *dt* in (2.28). Every vortex sheet element which moves beyond a boundary at a distance of four times δ_{dif} from the solid surface, is replaced with an equivalent vortex blob of the core spreading model, where the total circulation of the blob is equal to that of the original nascent vortex sheet, and the core radius is equal to the diffusion thickness.

2.5 Discrete Vortex Model

According to the generalized Biot-Savart law (2.18) or (2.19), it is known that the flow velocity is consisting of the vorticity induced velocity and the potential flow velocity, which respectively correspond to the first term of spatial integration and the second term of surface integration on the right hand side of the equation. Therefore, discretization of the vorticity field is one of the most important procedures for numerical calculation of velocity in the vortex methods.

If we represent the vorticity field with a mass of discrete vortices and introduce a local distribution of vorticity ω_{0i} as the i.th discrete vortex, we may rewire the term of spatial integration in (2.18) or (2.19) as

$$\frac{1}{\alpha}\int_V \frac{\omega_0 \times \mathbf{R}}{\mathbf{R}^\beta} dV_0 = \sum_i u_i \tag{2.29}$$

here,

$$u_i = \frac{1}{\alpha}\int_V \frac{\omega_{0i} \times \mathbf{R}}{\mathbf{R}^\beta} dV_0 \tag{2.30}$$

In the past studies, various models of vortex particles were proposed and tested, in which a discrete vortex has own smoothed vorticity distribution ω_{0i} and a core radius ε_i. For two-dimensional flow, Kuwahara and Takami [23] proposed a vortex blob whose core expands with time to simulate the viscous diffusion of vorticity. Chorin and Bernard [24] also proposed a blob, which was, however, a vortex with an invariable core size. For three-dimensional flow, Shriyama proposed a vortex stick which had a shape of a circular cylinder with a time dependent core, and Saffman and Meiron used a vortex ball called a vorton or a blob whose core remains invariant with time [2]. When applying the Biot-Savart law method to practical problems, one may consider that the vortex blob model offers rather simple procedure both in discretization of vorticity layers and in expression of viscous diffusion. For the, three-dimensional flow simulation in this study, the modeling by vortex blob is discussed hereinafter, where each blob has own smoothed vorticity distribution ω_{0i} and a core of radius ε_i.

In the case of two-dimensional flow, the Gaussian distribution of vorticity was examined by Leonard [3], which is represented

$$\omega_{0i} = \frac{\omega_i ds_i}{\pi \varepsilon_i^2} \exp\left(-\frac{\mathbf{R}^2}{\varepsilon_i^2} \right) \tag{2.31}$$

where, ω_i denotes the representative vorticity of the blob. Thus, substituting (2.31) and (2.30), the velocity induced by the above vorticity distribution can be represented as

$$u_i = \frac{\Delta\Gamma_i \left(k \times \mathbf{R} \right)}{2\pi \mathbf{R}^2} \left(1 - \exp\left(-\frac{\mathbf{R}^2}{\varepsilon_i^2} \right) \right) \tag{2.32}$$

here, $\Delta\Gamma_i k = \omega_i ds_i$, k: unit vector.

On the other hand, in case of three-dimensional flow, the spherically symmetric distribution of vorticity called a vortons was developed by Winckelmans and Leonard as referred to in [2]. The distribution function and the resultant induced velocity are represented by

$$\omega_{0i} = \frac{\alpha_i}{\varepsilon_i^3} f\left(x \right), \qquad u_i = \frac{\alpha_i \times \mathbf{R}}{4\pi R^3} g\left(x \right) \tag{2.33}$$

here,

$$f\left(x \right) = \frac{15}{8\pi} \frac{1}{\left(x^2 + 1 \right)^{7/2}}$$

$$g\left(x \right) = 4\pi \int_0^x t^2 f\left(t \right) dt = \frac{5x^3 + 2x^5}{2\left(x^2 + 1 \right)^{5/2}}$$

$$x = \frac{\mathbf{R}}{\varepsilon_i}$$

$$\alpha_i = \frac{4}{3} \pi \varepsilon_i^3 \omega_i \text{ (vortex strength).}$$

In order to take account of the viscous diffusion expressed by the third term on the right hand side of (2.23), the core spreading method is approximately introduced into the blob model, which is based on the exact solution of the Navier Stokes equation

for viscous diffusion of an isolated two dimensional vortex filament in a fluid at rest fluid, and the rate of core spreading is represented by

$$\frac{d\varepsilon_i}{dt} = \frac{c^2 \nu}{2\varepsilon_i} \tag{2.34}$$

here, c=2.242.

Since the total circulation is considered to be conserved in the transverse section of a vortex blob (Kelvin's theorem), the relation between the core radius ε_i and the representative vorticity ω_i can be given by $\omega_i \varepsilon_i^2 = const$. Therefore, the variation of the representative vorticity due to the viscous diffusion can be expressed as

$$\frac{d\omega_i}{dt} = -\frac{2\omega_i}{\varepsilon_i}\frac{d\varepsilon_i}{dt} \tag{2.35}$$

It should be noted here that although the accuracy of the core spreading method was criticized by Greengard, the convergence of the method to the solution of vorticity equation at least for some finite time has been confirmed by Cottet and by Nakajima and Kida as referred to in [2]

In recent studies, the core spreading equation (2.34) has been conveniently used for either two or three-dimensional flow. However, the vorticity transport due to the flow convection expressed by the second term on the right hand side of (2.23) should also be considered. Recently, Nakanishi et al [9] extended the spherical vortex blob model in order to take account of the longitudinal elongation of the vortex blob, in addition to the transverse diffusion due to viscosity. In either vortex model, a spherical vortex blob is tentatively replaced by an equivalent cylindrical vortex stick in the consideration of the longitudinal elongation and the stick elongated and diffused during a small time interval is replaced again by a new equivalent spherical blob with a different core radius. However, when the engineering application of the vortex method is considered, this scheme seems to be much complicated and the relation between the vorticity transport equation (2.23) and the variation of the core radius is not clear. As a simpler way to take account of the effect of convective motion on the core radius of a three dimensional vortex blob, one can obtain a scheme to easily evaluate the variation of the core radius from the approximate expression of the vorticity transport (2.23), considering the variation of vorticity due

to the viscous diffusion expressed by (2.34). In (2.23), if a position r_0 is taken at a center of a vortex blob, the vorticity ω_0 can be replaced by the representative vorticity of the blob ω_i, and the third term which means the rate of viscous diffusion of the vorticity can be expressed by (2.34) and (2.35). Then, one can derive

$$\omega_{i(t+dt)} = \omega_{i(t)} + (\omega g \nabla)_0 \, u_0 dt - \frac{\nu c^2 \omega_{i(t)}}{\varepsilon^2_{i(t)}} dt \tag{2.36}$$

Once the representative vorticity at $(t+dt)$ is evaluated from (2.36), the new core radius is calculated from the following equation based on the Kelvin's theorem.

$$\omega_{i(t+dt)} \varepsilon^2_{i(t+dt)} = \omega_{i(t)} \varepsilon^2_{i(t)} \tag{2.37}$$

From the above consideration, it has been clarified that when the core spreading method is applied to spherical vortex blob, the variation of vortex core during a small time interval is approximately estimated from consideration of both viscous diffusion and three-dimensional convective motion.

2.6 Diffusion Model of Vortex Blob

If the *i*-th vortex blob located r_i has a representative vorticity ω_i, a volume dv_i and a cut-off radius ε_i, the vorticity distribution of the *i*-th vortex blob is written by

$$\omega_{(\mathbf{r})} = \frac{1}{\varepsilon_i^{\,3}} p\left(\frac{|\mathbf{r}-\mathbf{r}_i|}{\varepsilon_i}\right)\omega_i dv_i \tag{2.38}$$

where $dv_i = \frac{4}{3}\pi\varepsilon_i^{\,3}$, and $\mathbf{P}_{(\rho)}\ p(\rho)$ is a radially symmetric smoothing function proposed by Winckelmans and Leonard as follows.

$$\mathbf{P}_{(\rho)} = \frac{15}{8\pi}\frac{1}{(\rho^2+1)^{7/2}} \tag{2.39}$$

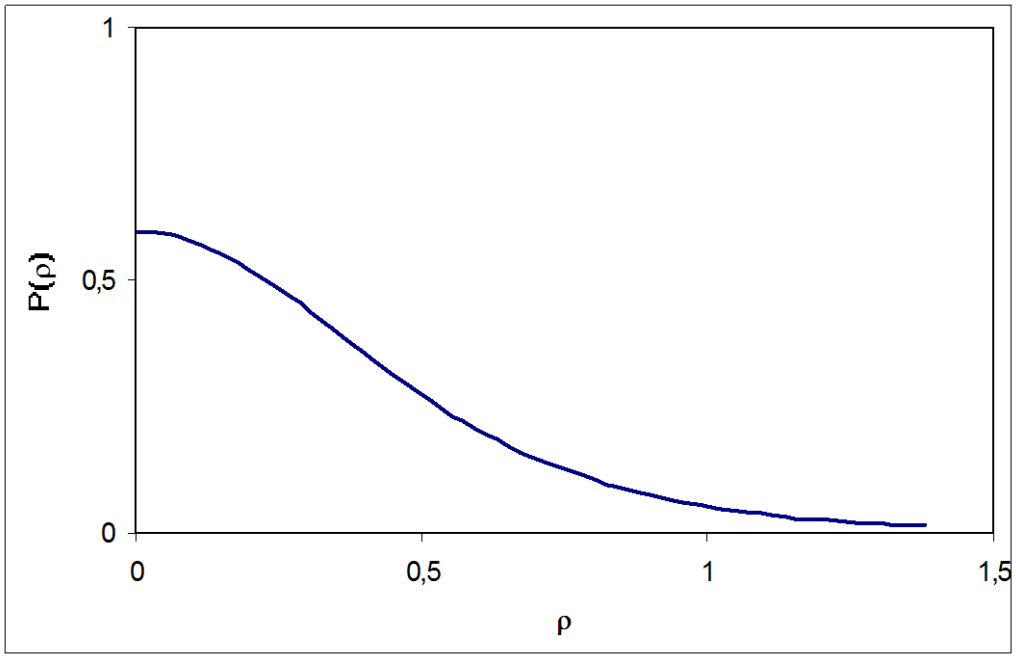


Figure 2.3: Radially symmetric smoothing function $p_{(\rho)}$.

Figure 2.3 shows the distribution function determined by equation (2.39). Then, velocity at an arbitrary point r in a flow field induced by all the blobs is given by the Biot-Savart law as follows:

$$\mathbf{u}_{(\mathbf{r})} = \frac{1}{4\pi}\sum_i \frac{\mathbf{w}_i \times \mathbf{R}}{R^3} q_{\left(\frac{R}{\varepsilon_i}\right)} dv_i \tag{2.40}$$

Where,

$$\mathbf{R} = \mathbf{r} - \mathbf{r}_i, \; R = |\mathbf{r} - \mathbf{r}_i|$$

$$q_{(\rho)} = 4\pi \int_0^{\rho} t^2 p_{(t)} dt,$$

The vortex blobs are allowed to flow at their own velocity consisting of the uniform approach velocity and the velocities induced by all the source panels and the blobs during a small time interval Δt. The movement of the blobs is calculated as integration of the velocity by the first order Euler scheme.

The variation of vorticity distribution of the i-th vortex blob depends on the vorticity transportation and the viscous diffusion effect. Now, it is supposed that the volume enclosed by cut-off radius as shown in Figure 2.3 varies that during small time interval due to the vorticity transportation and the viscous diffusion effect as shown Figure 2.4.

The change of representative vorticity of the i-th blob due to the vorticity transportation is determined by a vorticity equation, whose viscous term is omitted as follows,

$$\begin{aligned} \frac{D\mathbf{w}_i}{Dt} = \frac{1}{8\pi} \sum_j \times \left[\mathbf{w}_i \frac{2R_{ij}^2 + 5\varepsilon_j^2}{\left(R_{ij}^2 + \varepsilon_j^2\right)^{5/2}} - 3\mathbf{R}_{ij} \left(\mathbf{R}_{ij} \mathrm{g} \mathbf{w}_i\right) \frac{6R_{ij}^2 + 21\varepsilon_j^2}{\left(R_{ij}^2 + \varepsilon_j^2\right)^{7/2}} \right] \mathbf{w}_j dv_j \\ + \frac{1}{4\pi} \sum_k \int_{sk} \left[\frac{\omega_i}{R_{ik}^3} - \frac{3\mathbf{R}_{ik} \left(\mathbf{R}_{ik} \mathrm{g} \mathbf{w}_i\right)}{R_{ik}^5} \right] \sigma ds \end{aligned} \tag{2.41}$$

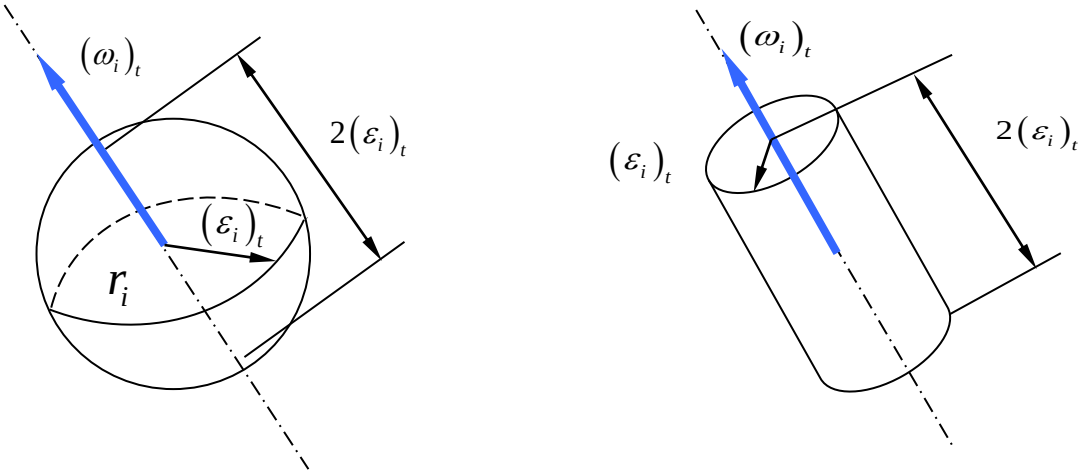


Figure 2.4: A radially symmetric vortex blob and its corresponding circular cylindrical stick.

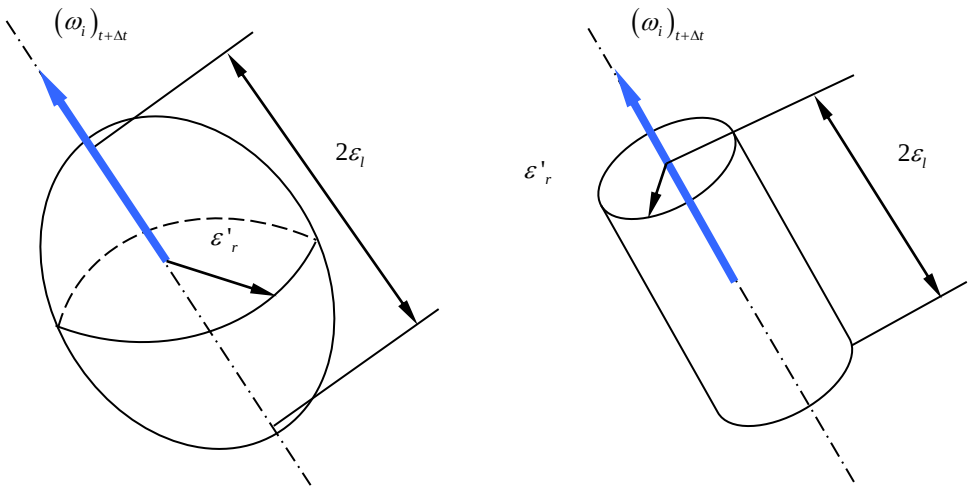


Figure 2.5: Stretching of vortex blob and its corresponding circular cylindrical stick.

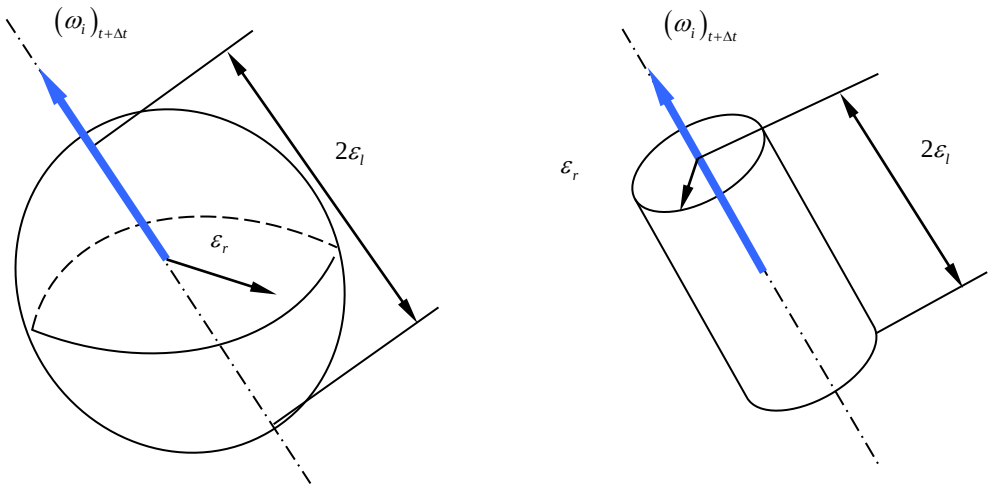


Figure 2.6: Diffusion of vortex blob and its corresponding circular cylindrical stick.

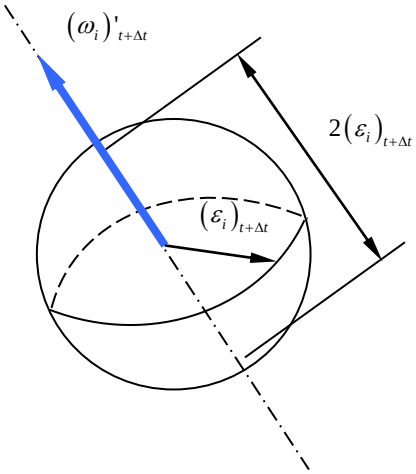


Figure 2.7: New vortex blob after stretching and diffusion.

Then, in order to determine ε_l, ε_r and ε'_r of Figure 2.5 and Figure 2.6, the blobs shown in Figure 2.4, 2.5 and 2.6 are replaced with corresponding circular cylinders. The cross sectional area of the cylinder corresponding to the blob shown in Figure 2.3 with its length parallel to the direction of the vorticity are given by $\pi\left(\varepsilon_i\right)_t^2$ and $2\left(\varepsilon_i\right)_t$ respectively. To find ε_l and ε'_r, one should use Kelvin and Helmholtz theorems respectively as:

$$\left(\omega_i\right)_{t+\Delta t}\left(\pi\varepsilon_{r'}^2\right)=\left(\omega_i\right)_t\left(\pi\varepsilon_i^2\right)_t \quad \left(Kelvin\,Theorem\right) \tag{2.42}$$

$$2\varepsilon_l\left(\pi\varepsilon_{r'}^2\right)=2\left(\varepsilon_i\right)_t\left(\pi\varepsilon_i\right)_t^2 \qquad \left(Helmholtz\,Theorem\right) \tag{2.43}$$

from (2.42) and (2.43) we can write ε_l as follows,

$$\varepsilon_l=\frac{\left(\omega_i\right)_{t+\Delta t}}{\left(\omega_i\right)_t}\left(\varepsilon_i\right)_t \tag{2.44}$$

for ε'_r, we can apply binomial expansion to (2.43) and

$$\varepsilon_{r'}=\left(\varepsilon_i\right)_t+\frac{1}{2}\left(\varepsilon_i\right)_t\frac{\left(\omega_i\right)_t-\left(\omega_i\right)_{t+\Delta t}}{\left(\omega_i\right)_{t+\Delta t}} \tag{2.45}$$

and, the change of the radius $\Delta\varepsilon_c$ on the cross section of the cylinder due to the vorticity transportation is given by

$$\Delta\varepsilon_c=\varepsilon_{r'}-\left(\varepsilon_i\right)_t \tag{2.46}$$

On the other hand, the change of the radius $\Delta\varepsilon_v$ on the cross section due to the viscous diffusion effect is assumed to be approximated by two-dimensional viscous diffusion for convenience. So, $\Delta\varepsilon_v$ is given by

$$\Delta\varepsilon_v=\frac{c^2\nu}{2\left(\varepsilon_i\right)_t}\Delta t \tag{2.47}$$

where, ν denotes kinematic viscosity of fluid, and the constant c is equal to 2.242 which can be obtained using an exact solution of Navier-Stokes equation for a straight and infinite long vortex filament in an unbounded fluid domain. Using, $\Delta\varepsilon_c$ and $\Delta\varepsilon_v$, ε_r shown in Figure 2.6. is determined to be:

$$\varepsilon_r = \left(\varepsilon_i\right)_t + \Delta\varepsilon_c + \Delta\varepsilon_v \tag{2.48}$$

If the blob shown in Figure 2.6. is now replaced with a new radially symmetric blob as in Figure 2.7. at time $t+\Delta t$ whose volume enclosed by cut-off radius being equivalent to that shown in Figure 2.6, a cut-off radius of new blob is given by

$$\left(\varepsilon_i\right)_{t+\Delta t} = \frac{2\varepsilon_r + \varepsilon_l}{3} \tag{2.49}$$

Since, the representative vorticity $\left(\omega_i\right)_{t+\Delta t}$ is calculated by equation (2.41) whose viscous diffusion term is omitted, the vorticity is improved by using the cut-off radius given by equation (2.49) as follows

$$(\omega_i)'_{t+\Delta t} = \left[\frac{\varepsilon'_r}{(\varepsilon_i)_{t+\Delta t}}\right]^2 (\omega_i)_{t+\Delta t} \tag{2.50}$$

2.7 Panel Method

In the panel method approach, the body surface is modeled by N small, flat, quadrilateral panels onto which singularities in the form of sources and/or vortexes are placed. Assume for illustration that only sources are used. If the source strength on the i^{th} "sending" panel is σ_i, then the velocity induced by this panel at the j^{th} control point on the "receiving" panel can be written as $K_{ij}\sigma_i$. K is called an influence coefficient, which depends on the geometry of the "sending" panel, the distance of the "receiving" control point from the panel, and the relative orientation of both panels. For the case where j=i, the influence coefficient is exactly 0.5. The velocity normal to the surface at the j^{th} control point induced by all of the N sources will be

$$v_j = \sum_{\substack{i=1 \\ i\neq j}}^{N} K_{ij}\sigma_i \tag{2.51}$$

The boundary condition of flow tangency is imposed at the centroids of each panel, along with a boundary condition describing the flow away from the body surface. Initially, the boundary condition is the free-stream flow at infinity. In this case, the

component of the free-stream velocity, $\vec{U}_\infty$, normal to the j^{th} panel will be $\vec{U}_\infty \cdot \vec{n}_j$, where $\vec{n}_j$ is the unit normal vector. Therefore, at the j^{th} panel:

$$\sum_{\substack{i=1 \\ i \neq j}}^{N} K_{ij}\sigma_i + \frac{\sigma_i}{2} + \vec{U}_\infty \cdot \vec{n}_j = 0 \tag{2.52}$$

One equation such as this applies at each of the N panels. This leads to a set of influence coefficients in the form of a set of linear simultaneous equations that can be used to solve for the singularity strengths (σ) using standard numerical methods. The governing equations can be written in matrix form as

$$\left[K_{ij}\right]\left\{\sigma_i\right\} = -\left\{\vec{U}_\infty \cdot \vec{n}_j\right\} \tag{2.53}$$

noting that the self-induced influence coefficient, $K_{ii} = 0.5$, runs along the diagonal of the [A] matrix. Once the σ_i s are obtained, the velocity components tangential to the panels can be obtained. Normally thousands of panels are required to adequately resolve a 3D body, especially in high curvature regions. Because the numerical cost of these panel methods is of order N^3, their use is by no means inexpensive, even on a modern computer.

It should be noted that, in this study the above described potential flow simulation around bluff bodies is followed by a separated flow simulation by means of shedding of surface panels into the flow field. Thus, the right hand side onset velocities at control points on bluff body surfaces are modified at each time step of separated flow evolution. However, the influence coefficient matrix on the left hand side is only function of surface geometry and therefore remains constant throughout the calculation. The coefficient matrix is calculated only once at the start of the separated flow calculation.

2.8 Calculation Procedure

Briefly, a typical application of the algorithm is as follows.

1. Read geometric data (or previously run data).
2. Build coefficient matrix, [K] which depends on surface geometry.
3. Calculate the normal velocities induced by the free stream velocity at control points and thus build the [RHS] vector.
4. Calculate source panel strengths, $[\sigma]$ from $[K]^{-1}$ and [RHS].
5. Evaluate induced velocity at panel corners.
6. Evaluate vorticity due to the induced velocity found in step 5.
7. Introduce vortex panels into flow-field.
8. Update the source-strengths to satisfy the no normal velocity condition.
9. Calculate the induced velocity at vortex panel corners and vortons
10. Move the vortex panels and vortons.
11. Change vortex panels to vortons, if panels are adequately away from the body.
12. Write flow-field data to output files.
13. Repeat steps 4 through 12 for the next time step.

3. RESULTS AND CONCLUSION

In this study, incompressible, viscous three-dimensional flows over a sphere, and a circular cylinder have been simulated using a discrete vortex approach described above. Simulations and characteristics of flow have been performed at various Re numbers.

3.1 Flow Simulation around a Sphere

The starting flow around a sphere is calculated at a Reynolds number $\mathrm{Re} = \frac{U_\infty D}{\nu} = 1000$. Re enters into the calculation as kinematic viscosity $\nu = \frac{U_\infty D}{\mathrm{Re}}$ in Eq. 2.45. The sphere is represented by 200 panels on which sources with linearly varying strength are distributed (Figure 3.1). The time interval is given as $\Delta t = 0.1\frac{D}{U_\infty}$, where, D denotes diameter of the sphere and U_∞ denotes free-stream velocity. Both of the initial cut-off radius and the introduction height h above the surface of the sphere are given as 0.05D. The flow around the sphere was calculated for the period of 0.0 to 9.0 of the non-dimensional time $T = \frac{t}{(D/U)}$. As evident from Figure 3.2 the vortex panels introduced above the surface of the sphere form a vortex ring just behind the sphere. Figure 3.3 and Figure 3.4 a-j shows the evolution of the flow pattern between T=0.0 and T=9.0. At T=9.0 the wake is no longer axially symmetric, it has completely three-dimensional structure.

In contrast to the flow patterns at T=4.0 and T=5.0 showing initial axisymmetric development of the separated flow, the flow pattern at T=9.0 demonstrates the formation of a spiral structure in the wake flow behind the sphere.

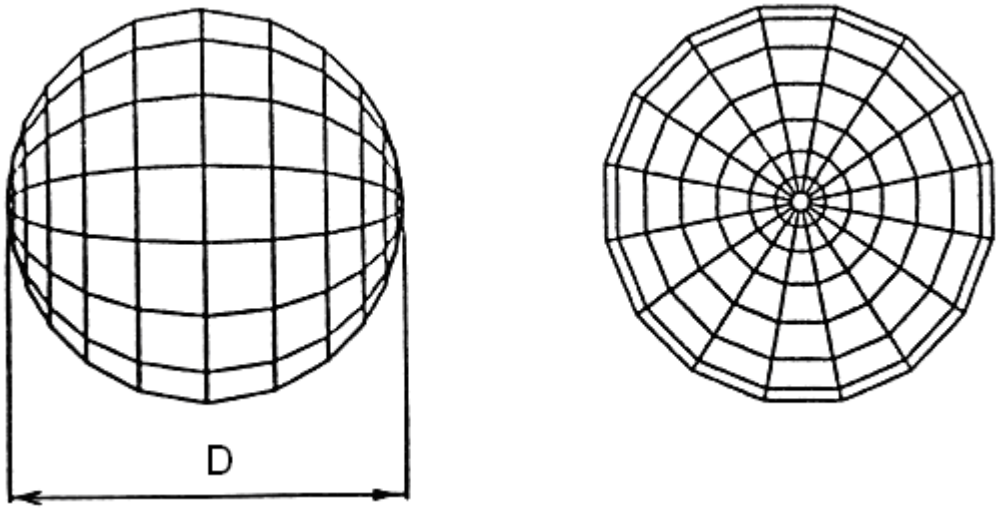


Figure 3.1: Panel configuration of sphere

Previously, Nakanishi and Kamemoto [9] calculated flow around sphere. In their study, the sphere is represented by 200 panels. Figure 3.2 and Figure 3.3 show their results at time T=2.0 and T=9.0.

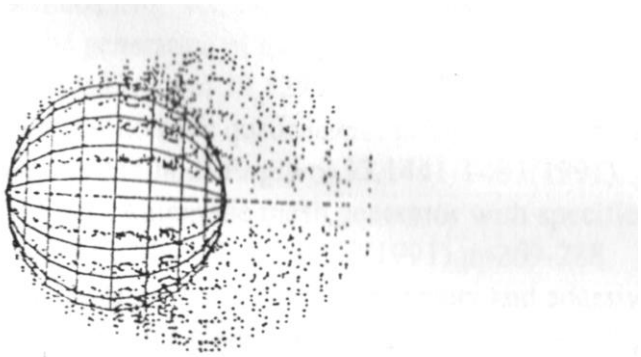
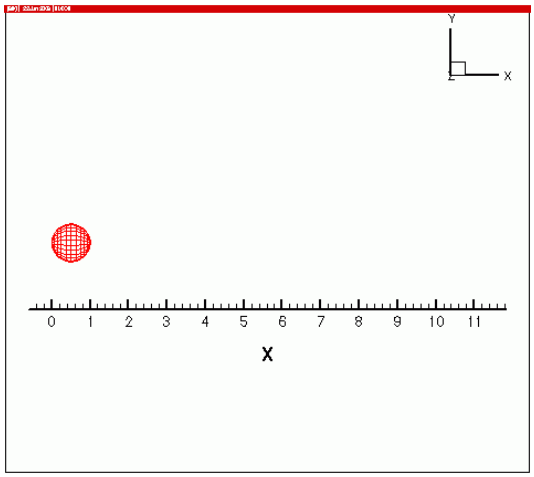


Figure 3.2: Flow pattern around sphere (T=2.0)

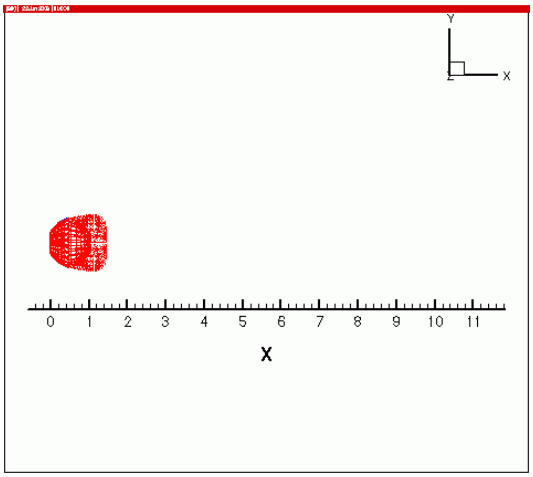


Figure 3.3: Flow pattern around sphere (T=9.0)

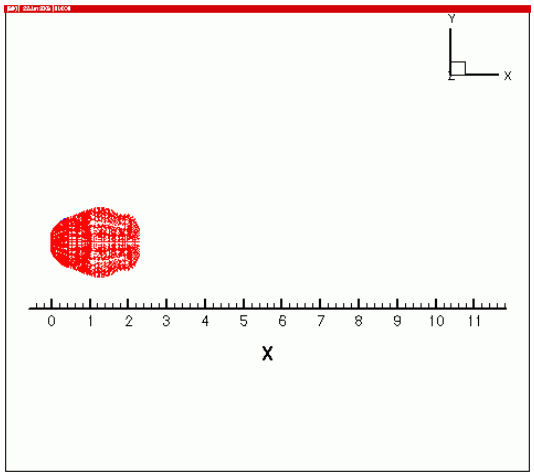
a)T=0.0



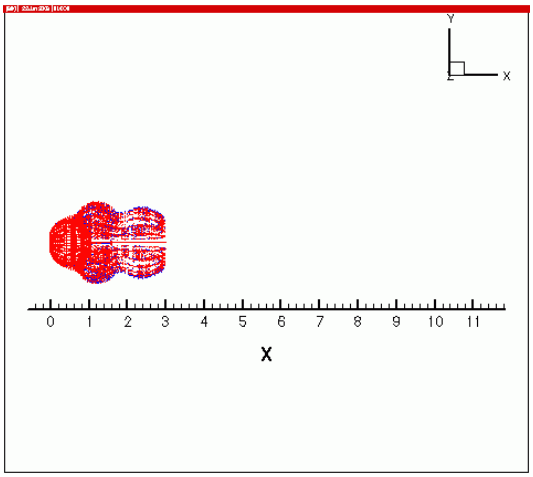
b)T=1.0



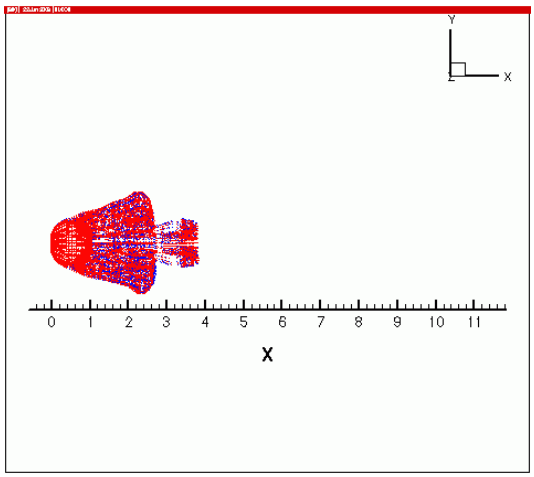
c)T=2.0



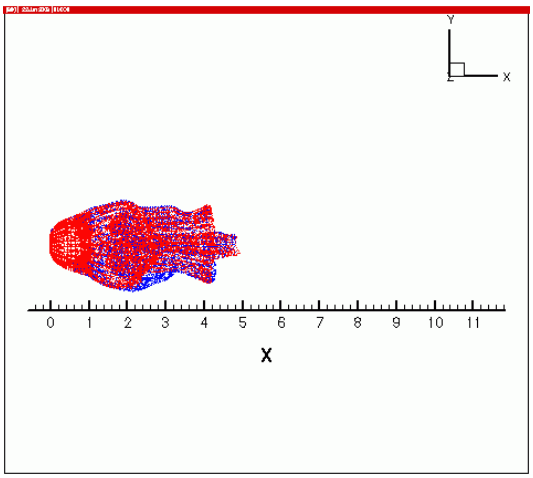
d)T=3.0



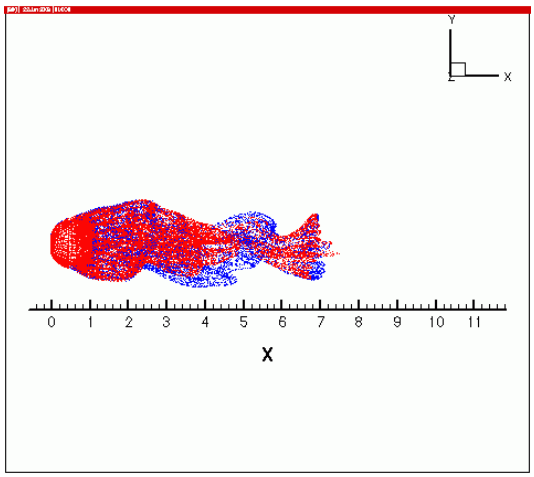
e)T=4.0



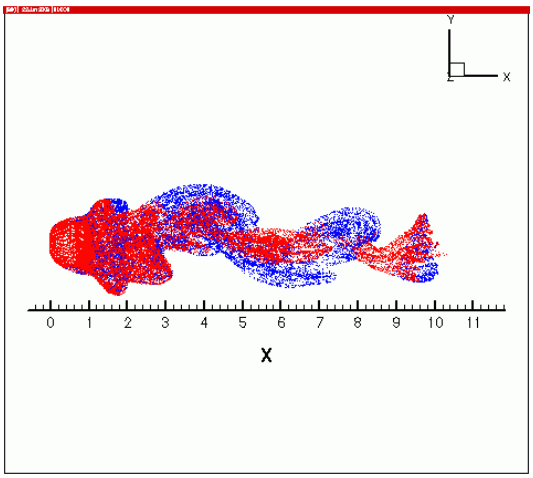
f)T=5.0



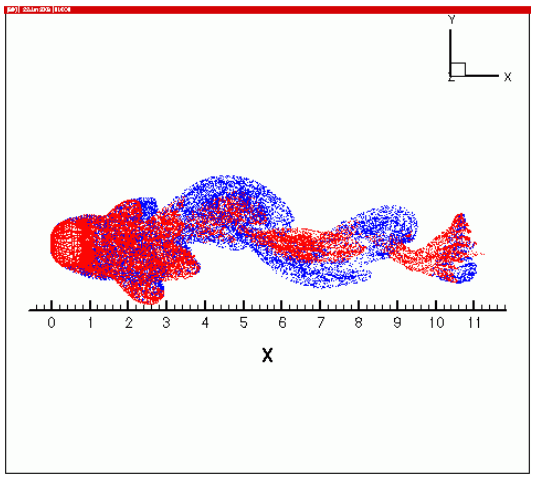
g)T=6.0



h)T=7.0



i)T=8.0



j)T=9.0

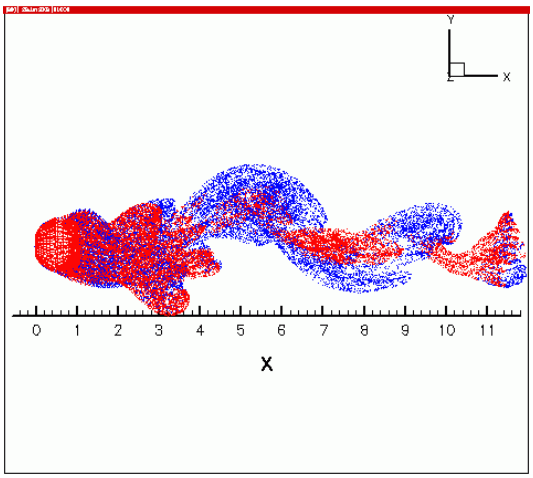
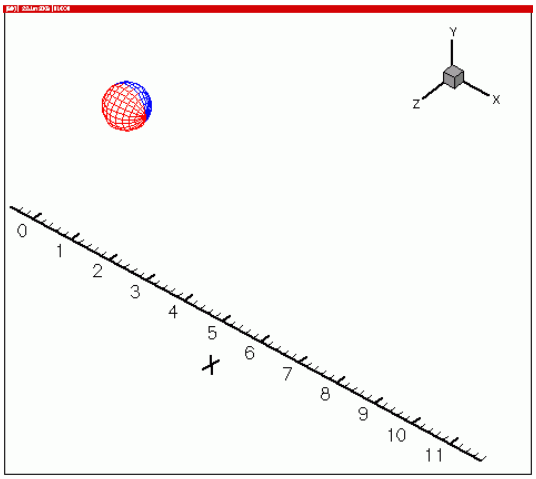
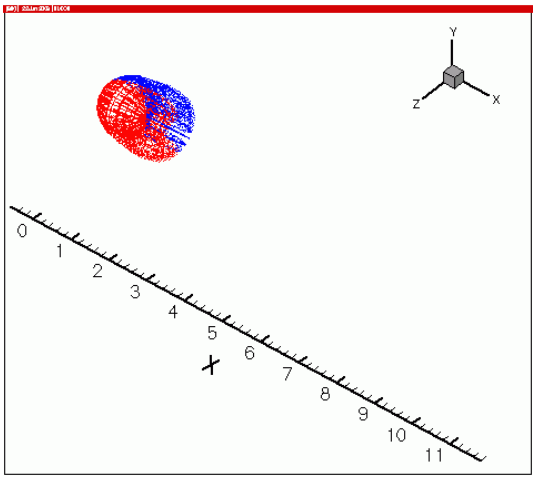


Figure 3.4: Side view of discrete vortex flow pattern around sphere at the elapsed times T=0, 1.0, 2.0, 3.0, 4.0, 5.0, 6.0, 7.0, 8.0, and 9.0 (Re=1000)

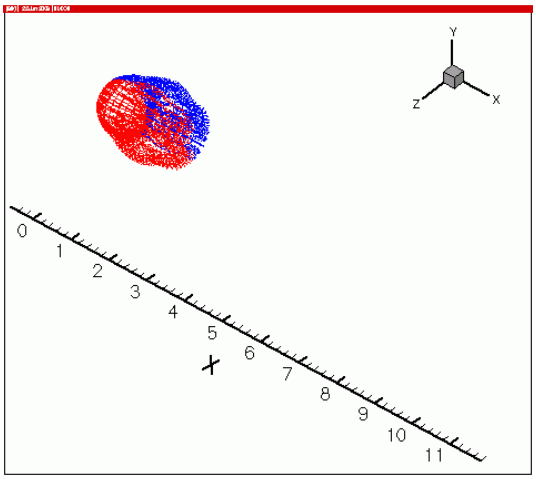
a)T=0.0



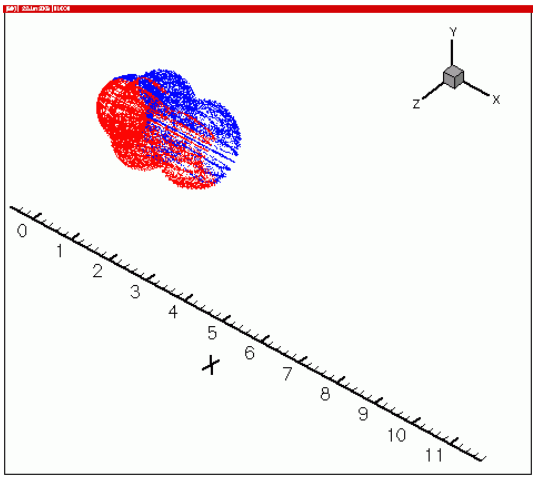
b)T=1.0



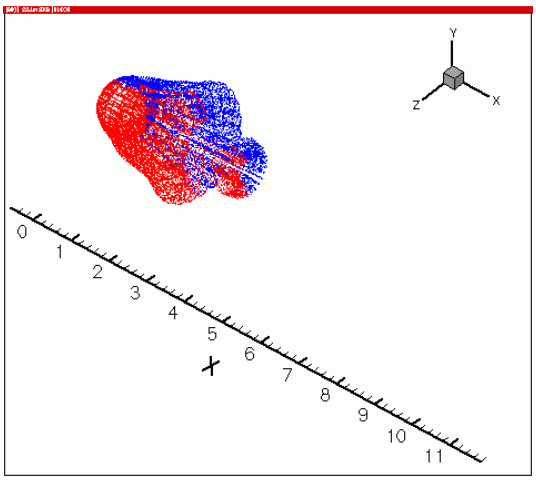
c)T=2.0



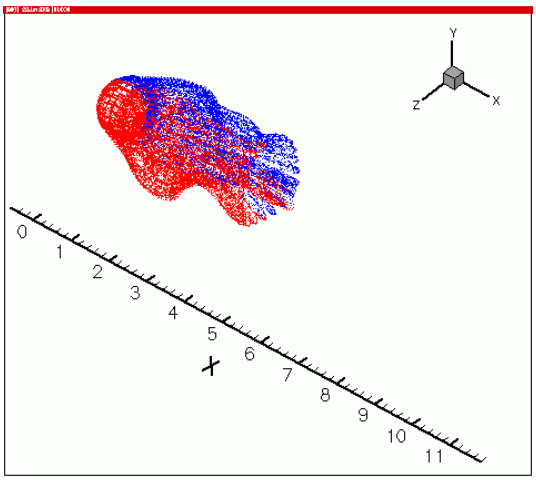
d)T=3.0



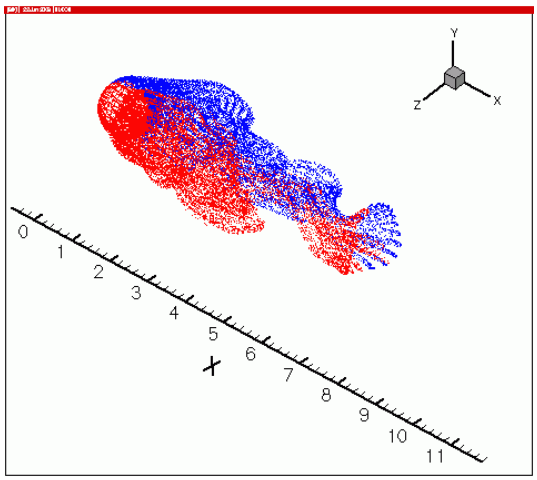
e)T=4.0



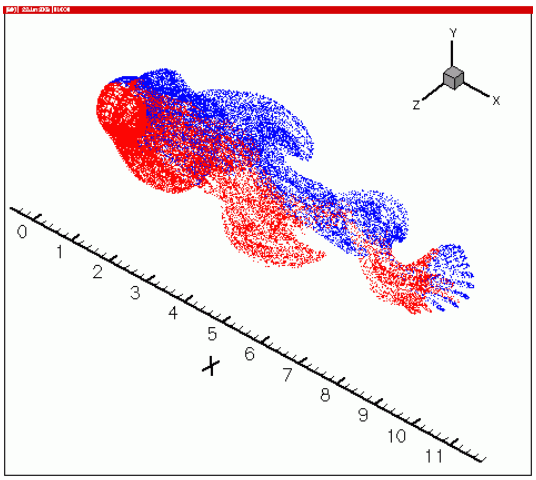
f)T=5.0



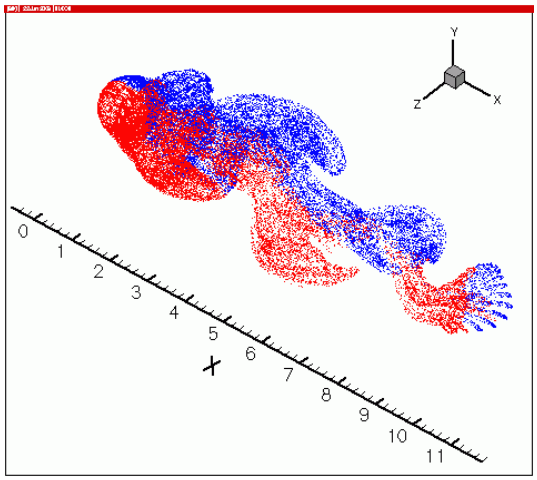
g)T=6.0



h)T=7.0



i)T=8.0



j)T=9.0

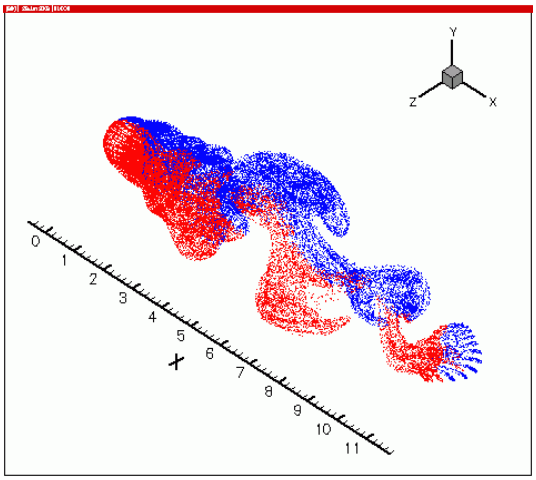


Figure 3.5: 3D discrete vortex flow patterns around sphere at the elapsed times T=0, 1.0, 2.0, 3.0, 4.0, 5.0, 6.0, 7.0, 8.0, and 9.0 (Re=1000)

3.2 Flow Simulation around a Circular Cylinder

Three-dimensional separated viscous flows around a circular cylinder have been calculated using a source panel method in combination with the Lagrangian discrete vortex method. Calculations have been performed at Re= 50, 200 and 500.

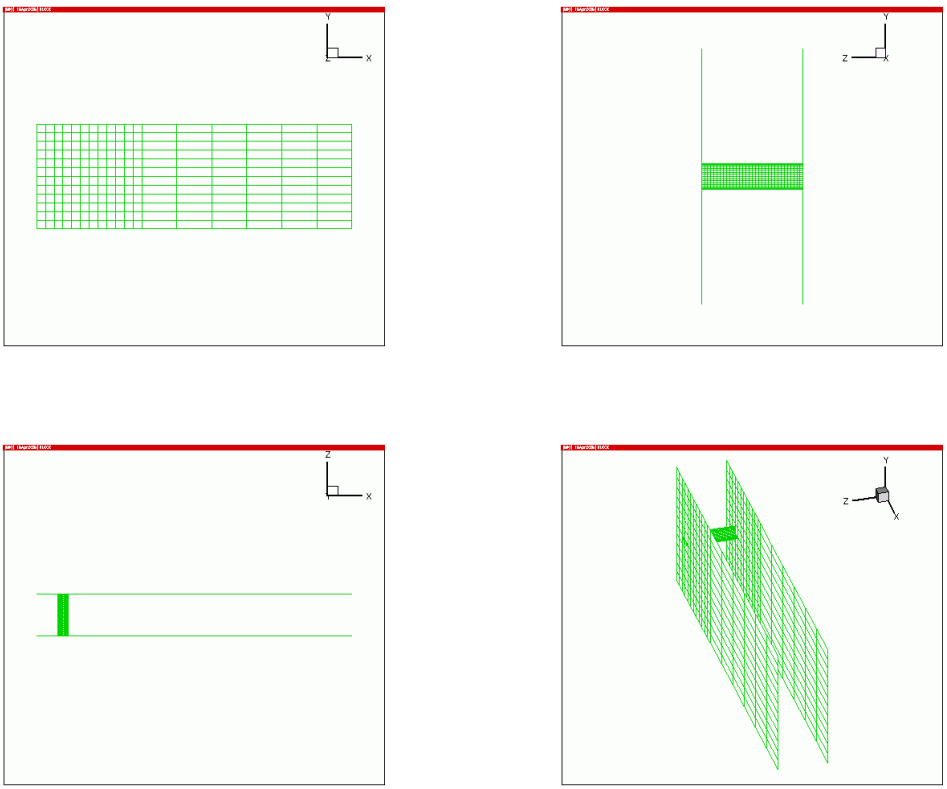


Figure 3.6: Views of circular cylinder and sidewalls

As shown in Figure 3.7, wake structure of circular cylinder (body 3) is investigated by also considering its images (body 2 and 4) with respect to sidewalls (bodies 5,6,7, and 8). The image bodies (2 and 4) are needed in order to enforce the periodicity at the cylinder ends and therefore to simulate the flow around an infinitely long cylinder.

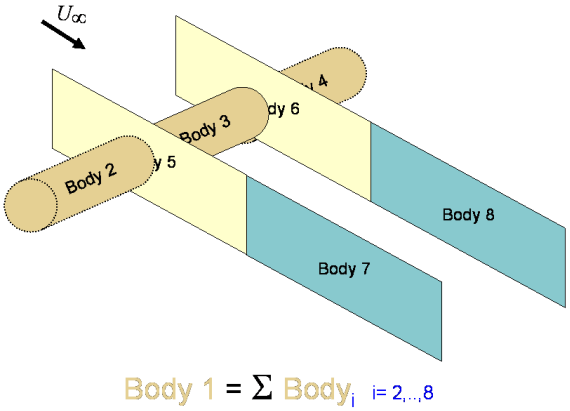


Figure 3.7: Calculated body, images of the body and side walls.

3.2.1 Run Parameters for the Circular Cylinder

In the representation of the cylinders (Figure 3.6) with rectangular panels, the number of division along the azimuthal and spanwise directions is 36. The parallel walls at both ends of the bodies extend from -2.5D to 27.5D and from -4D to 4D in x and y directions respectively. Each wall has 12 equal divisions in the y direction. In the x direction the part extending from -0.5D to 7.5D is equally divided into 12 whereas the rest has 6 divisions.

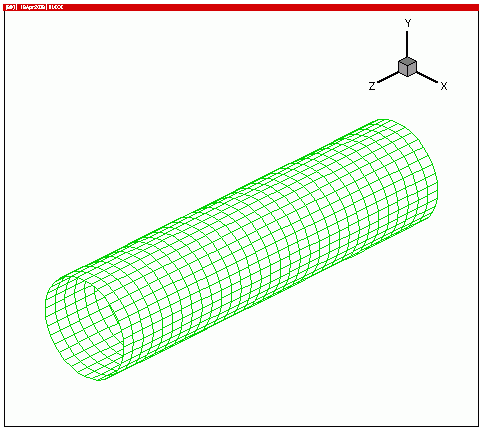
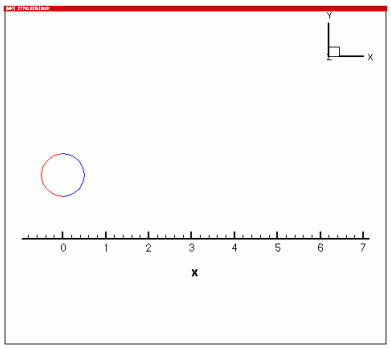


Figure 3.8: Perspective view of circular cylinder.

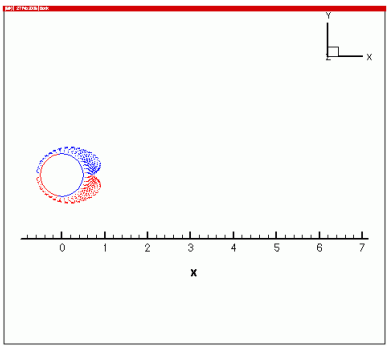
The bodies used in the investigation are represented with 1584 rectangular panels. For simulation of flow around a circular cylinder and its wake about 300.000 vortex elements are used. Parallel computing using MPI (Message Passing Interface) routines have been performed with a computer having 8x400 MHz IP35 processors and a memory size of 5120 MB. A typical computational time is order of a week.

3.2.2 Case 1 (Simulation at Re=50)

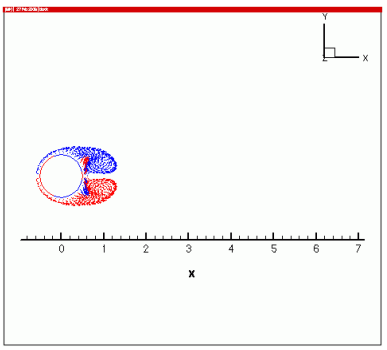
T=0.0



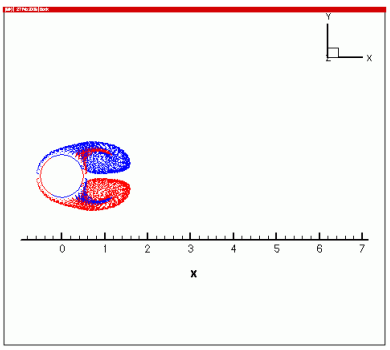
T=1.0



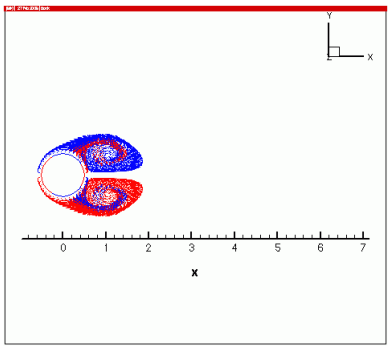
T=2.0



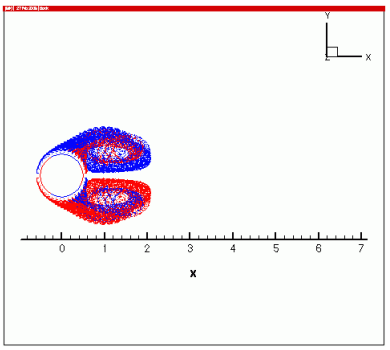
T=3.0



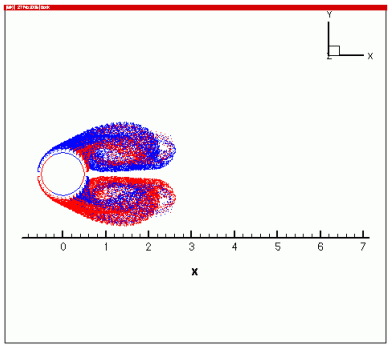
T=4.0



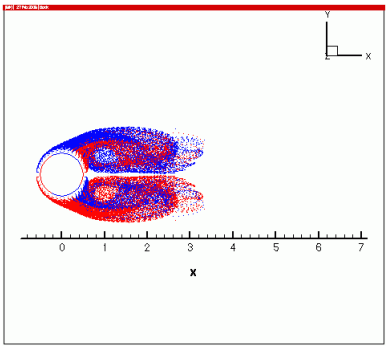
T=5.0



T=6.0



T=7.0



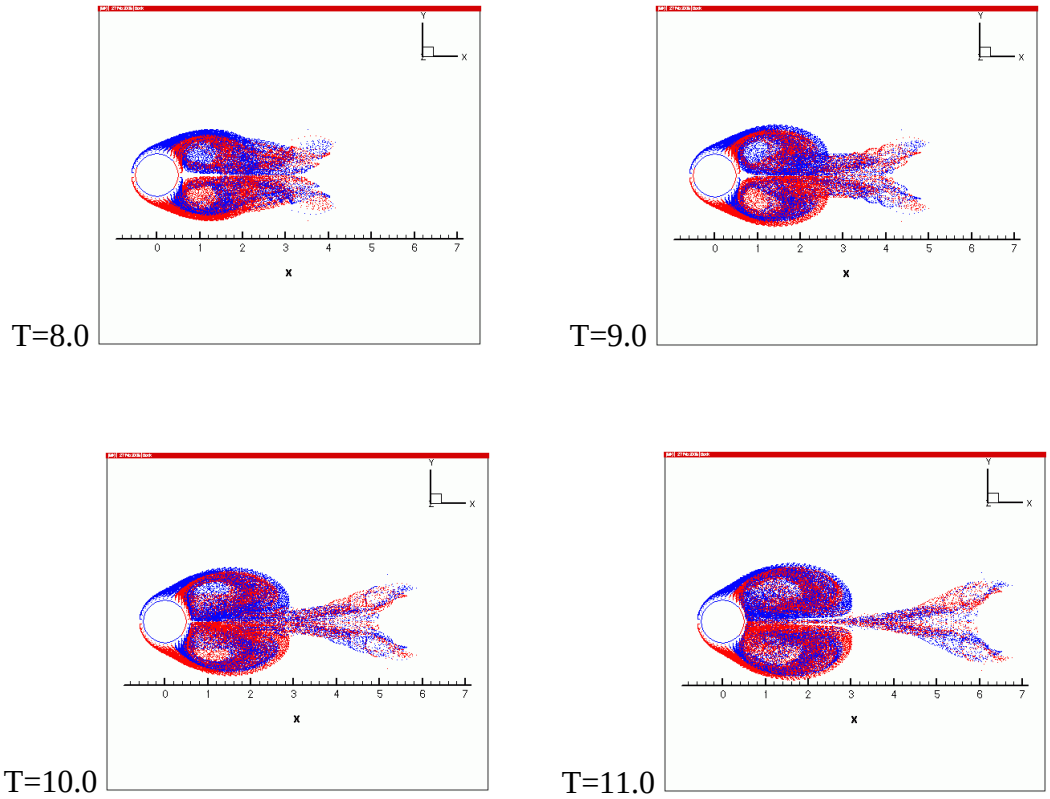
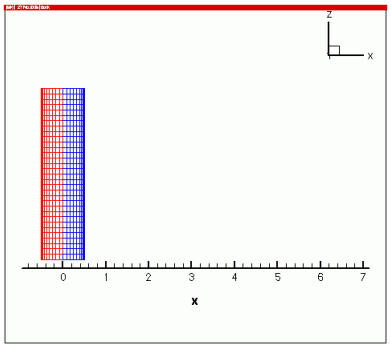
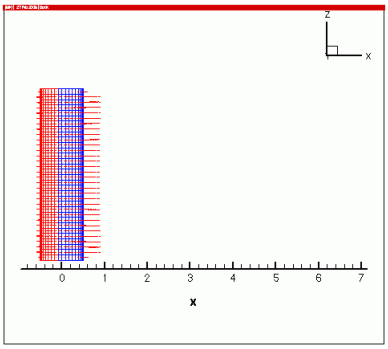
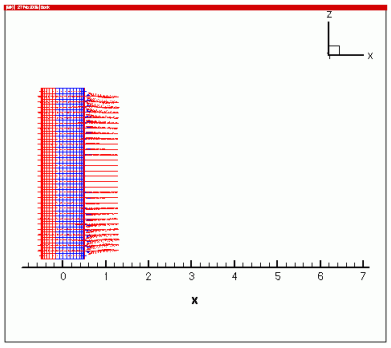
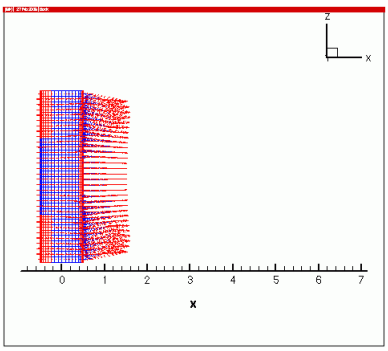


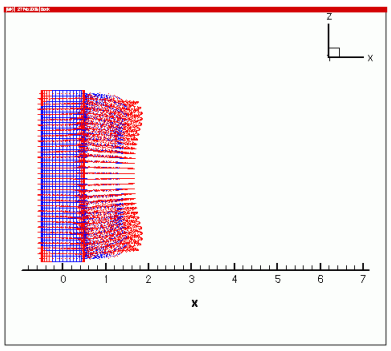
Figure 3.9: Wake structures of circular cylinder in xy plane from T=0.0 to T=11.0. Re=50

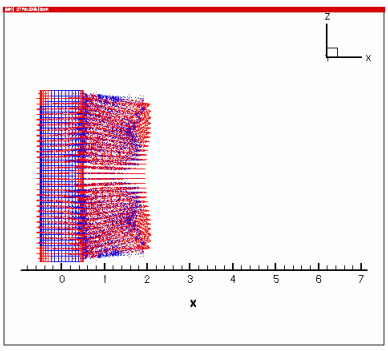
T=0.0 

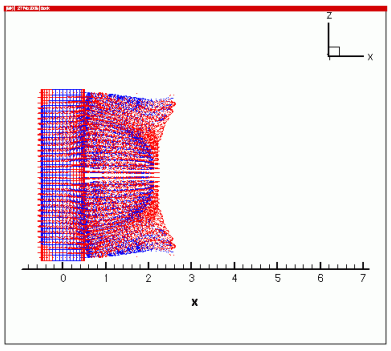
T=1.0 

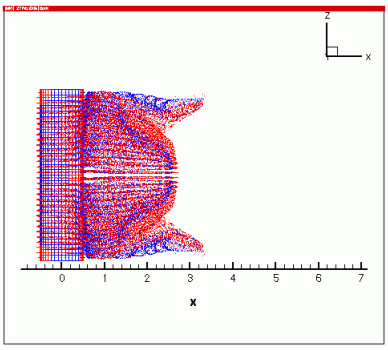
T=2.0 

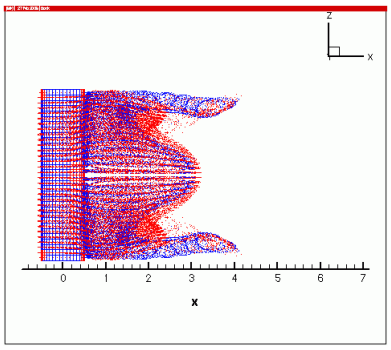
T=3.0 

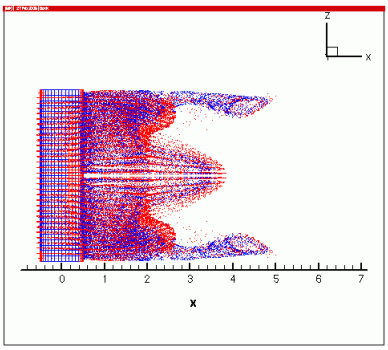
T=4.0 

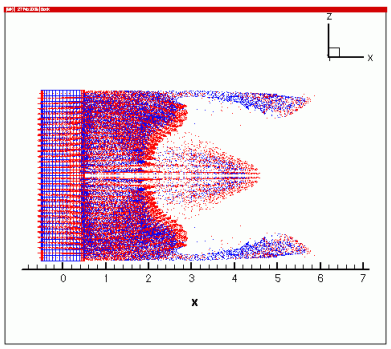
T=5.0 

T=6.0 

T=7.0 

T=8.0 

T=9.0 

T=10.0 

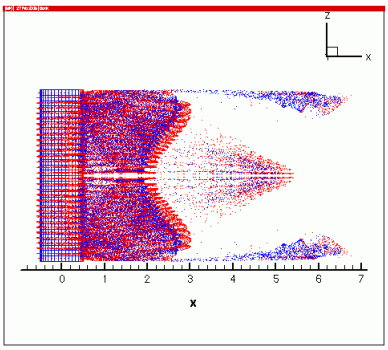
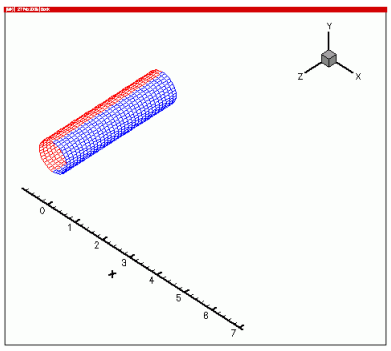
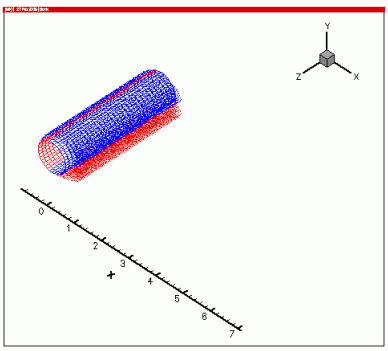
T=11.0 

Figure 3.10: Wake structures of circular cylinder in xz plane from T=0.0 to T=11.0. Re=50

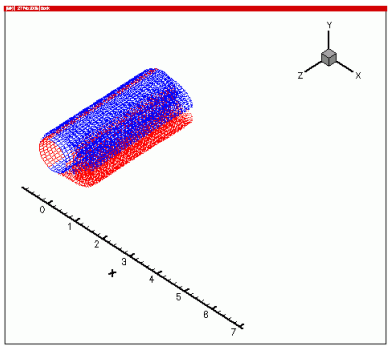
T=0.0



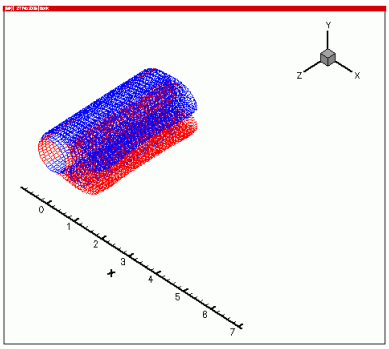
T=1.0



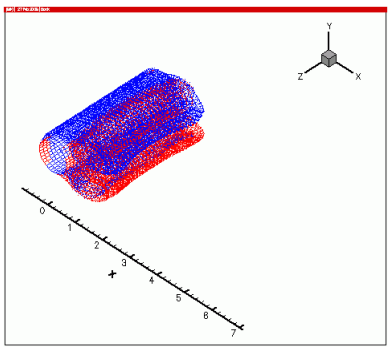
T=2.0



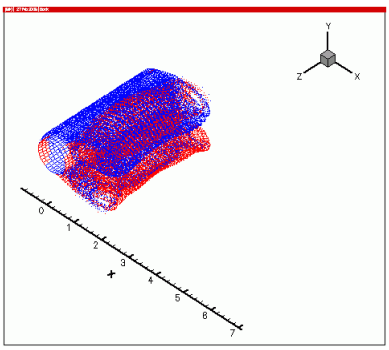
T=3.0



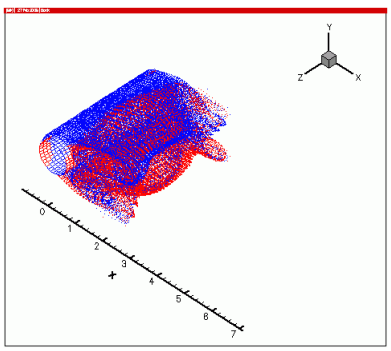
T=4.0



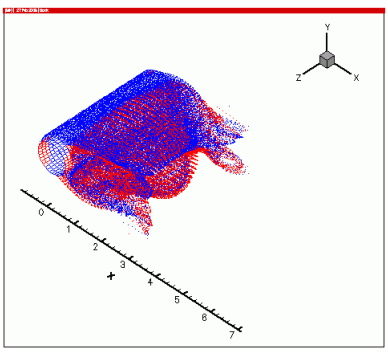
T=5.0



T=6.0



T=7.0



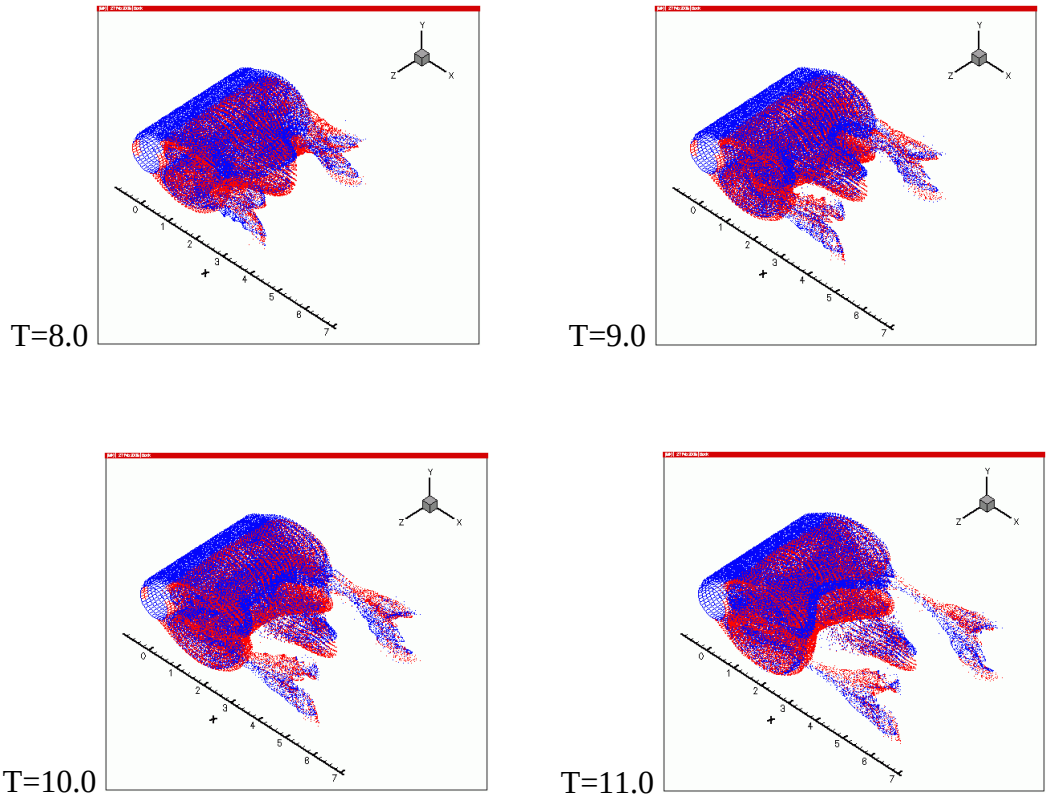


Figure 3.11: Perspective view of wake structures of circular cylinder from T=0.0 to T=11.0. Re=50

3.2.3 Case 2 (Simulation at Re=200)

3.2.3 Case 2 (Simulation at Re=200)

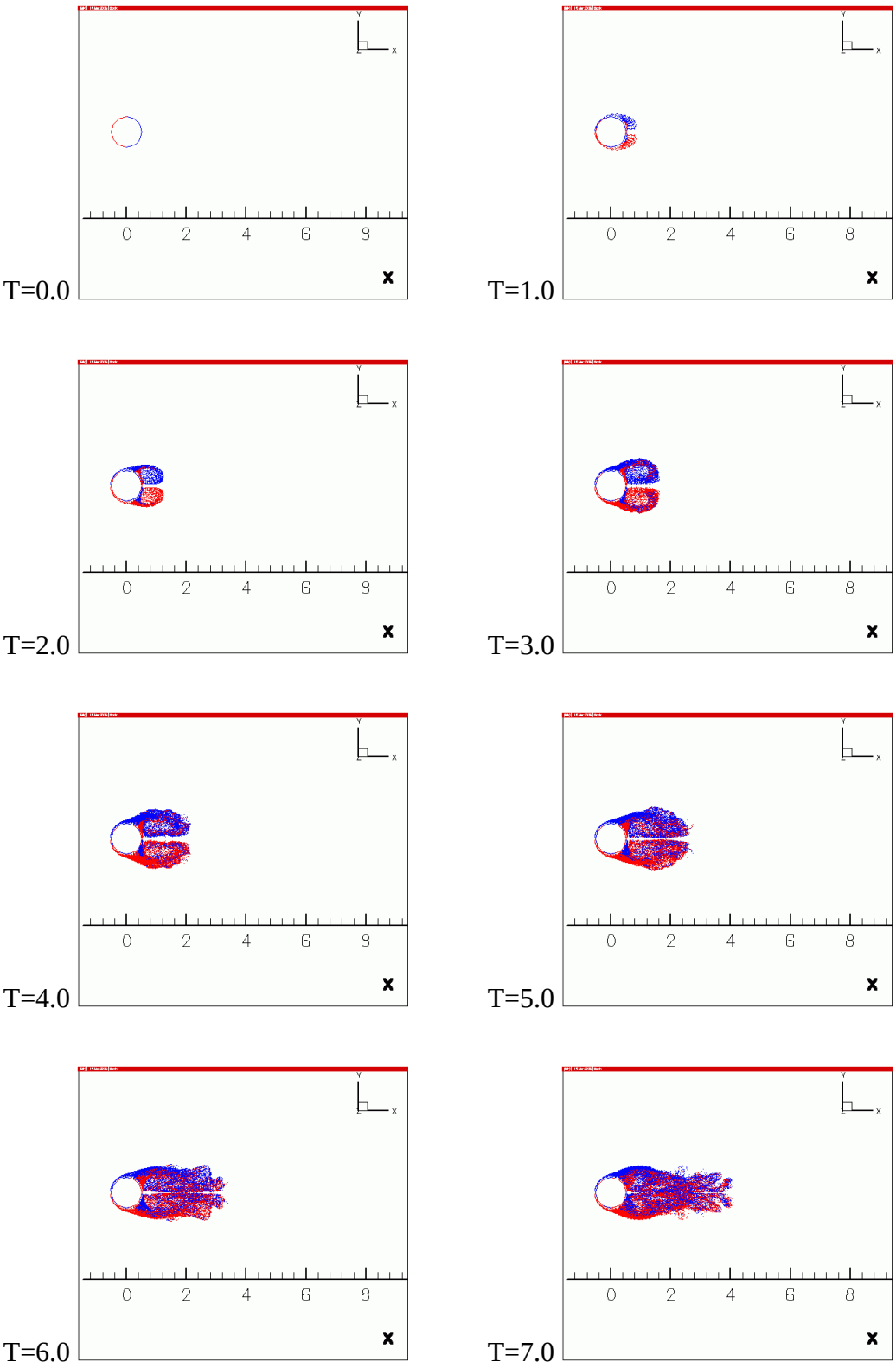


Figure 3.12: Wake structures of circular cylinder in xy plane from T=0.0 to T=7.0. Re=200

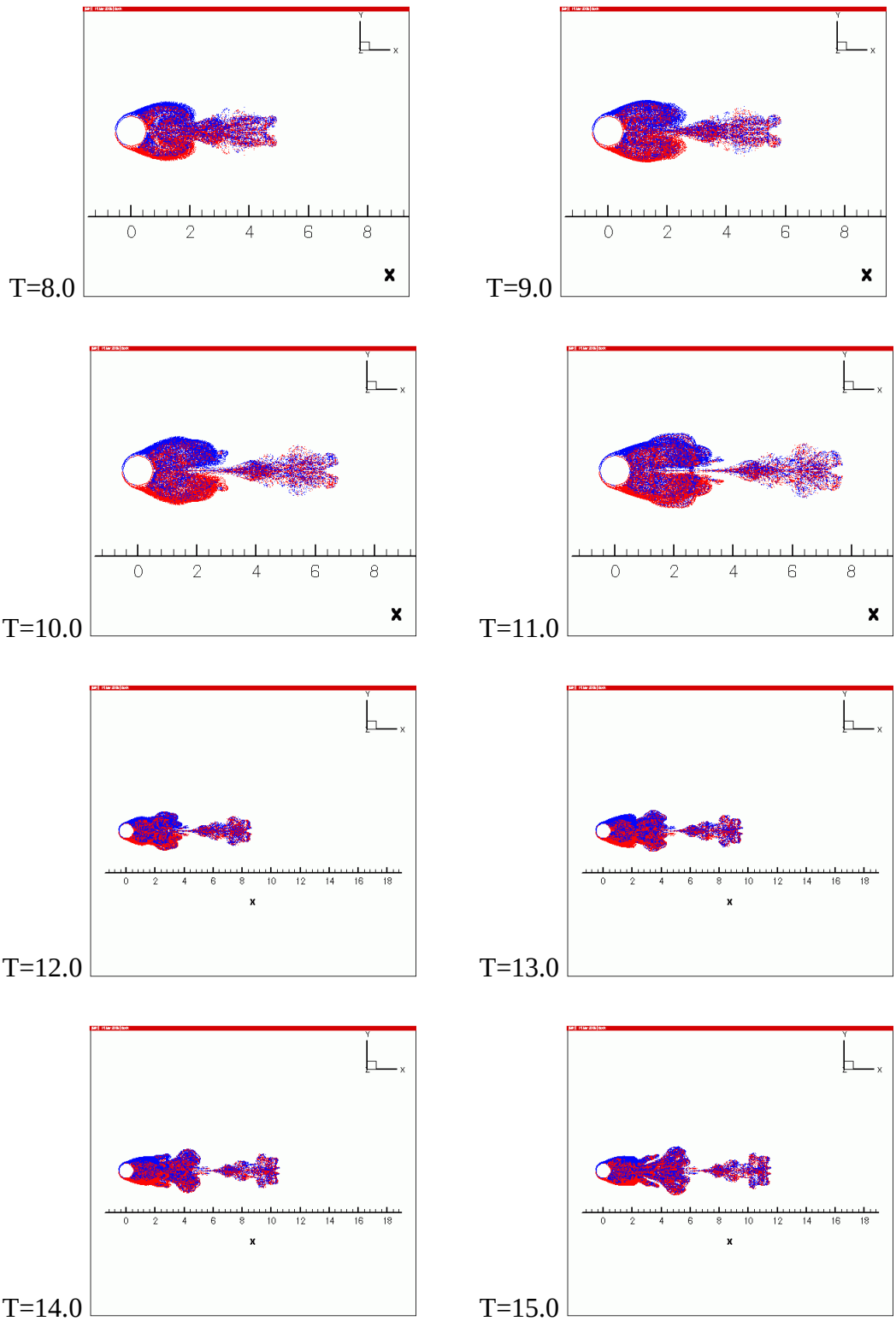


Figure 3.13: Wake structures of circular cylinder in xy plane from T=8.0 to T=15.0. Re=200

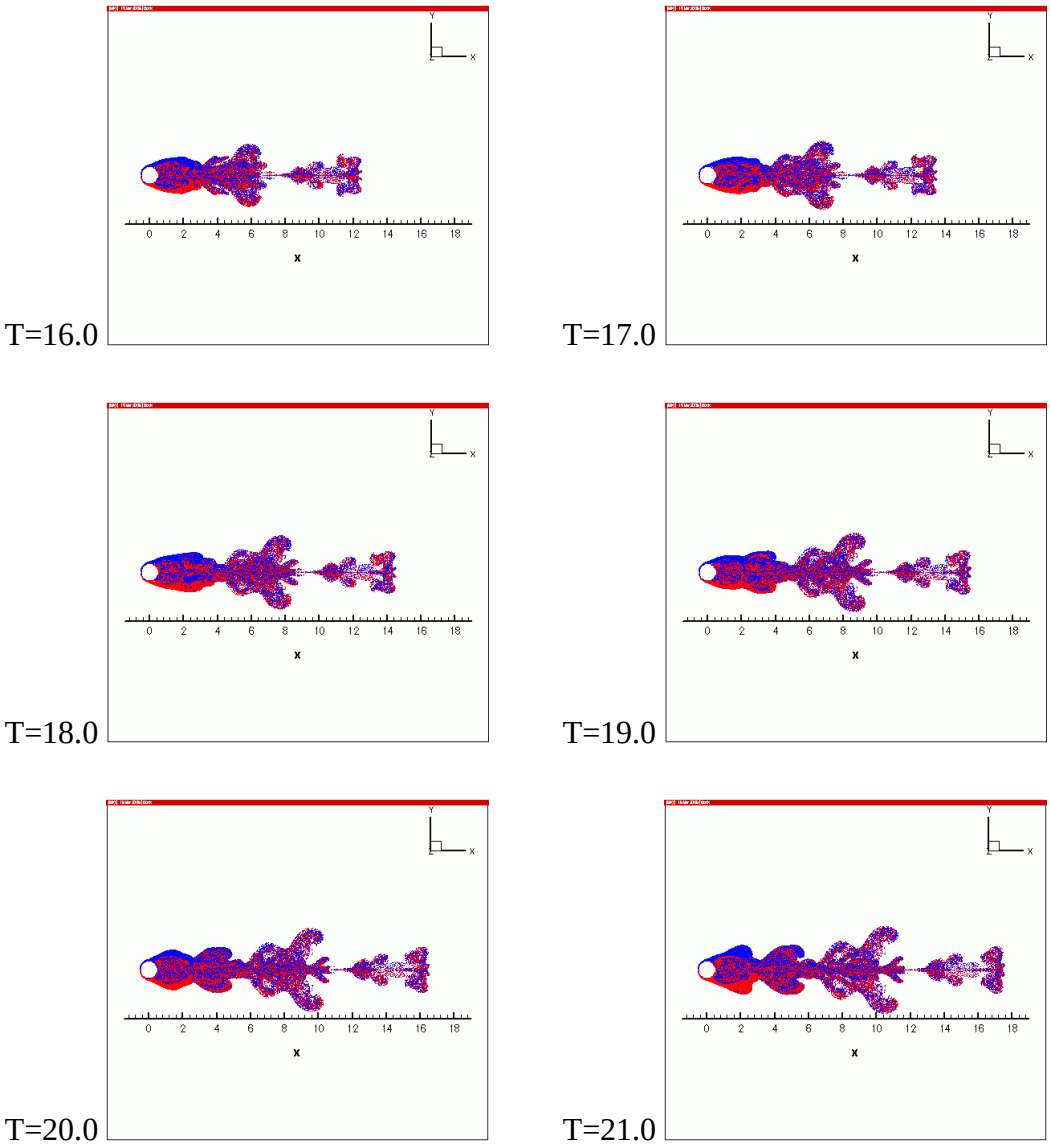


Figure 3.14: Wake structures of circular cylinder in xy plane from T=16.0 to T=21.0. Re=200

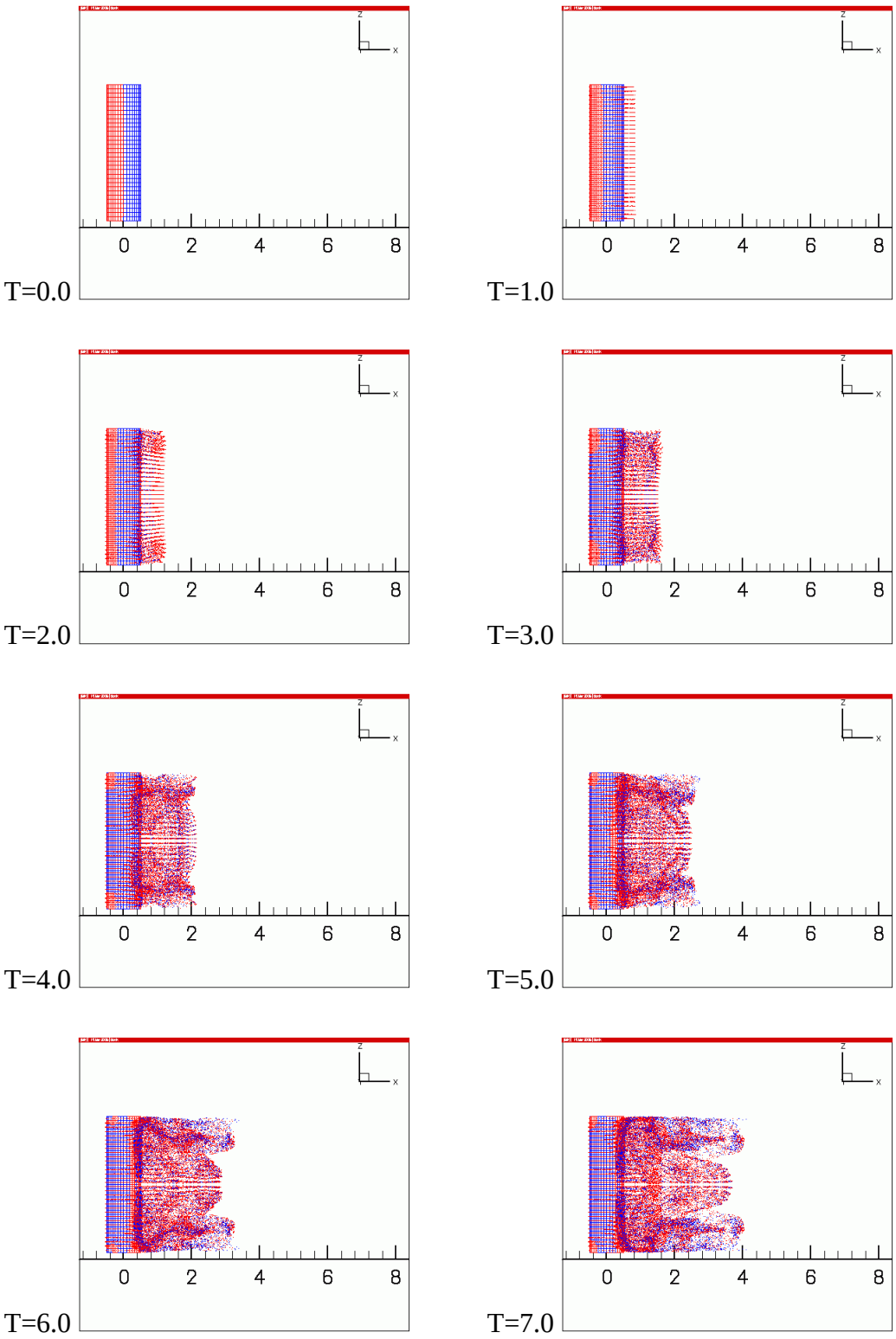


Figure 3.15: Wake structures of circular cylinder in xz plane from T=0.0 to T=7.0. Re=200

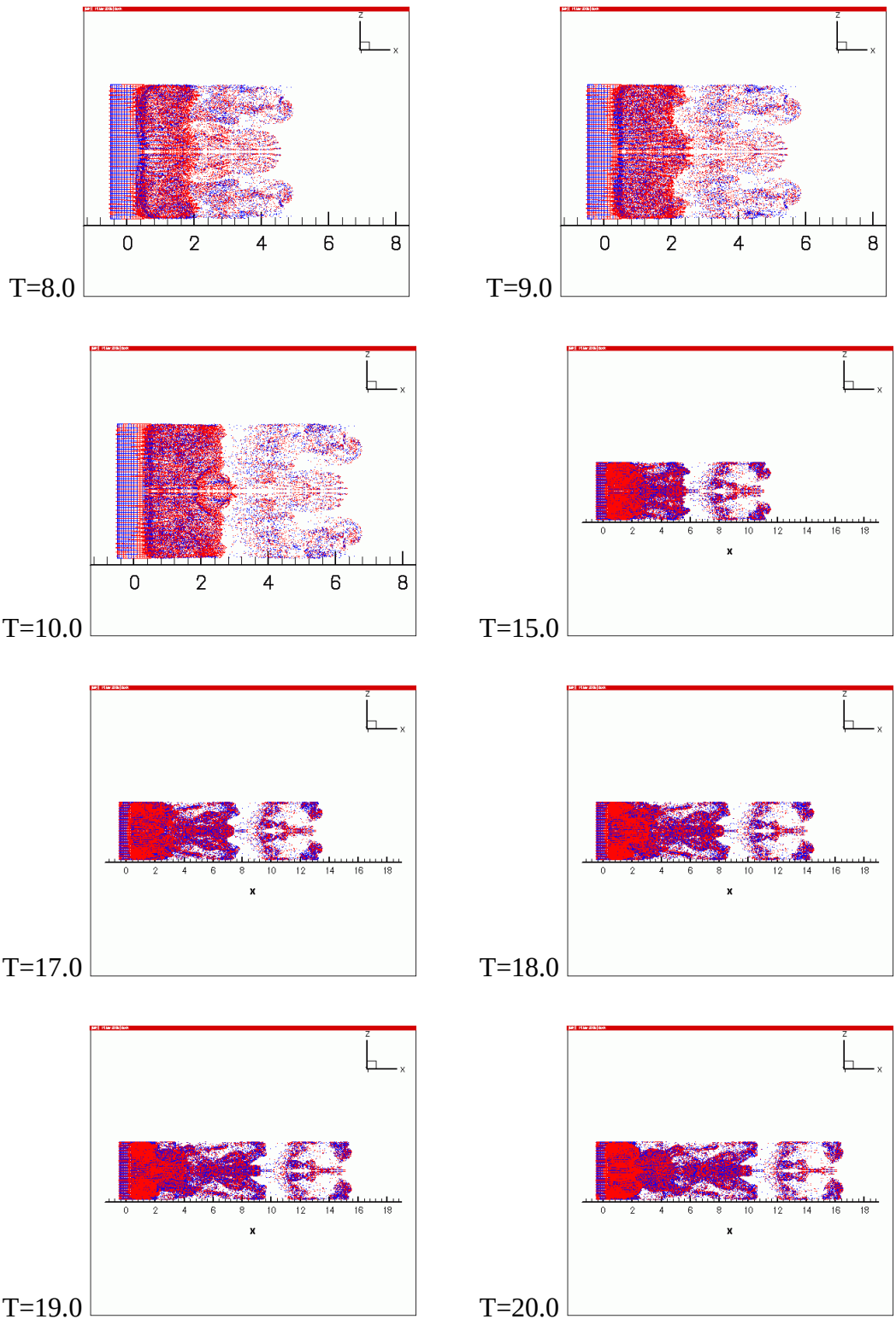


Figure 3.16: Wake structures of circular cylinder in xz plane from T=8.0 to T=20.0. Re=200

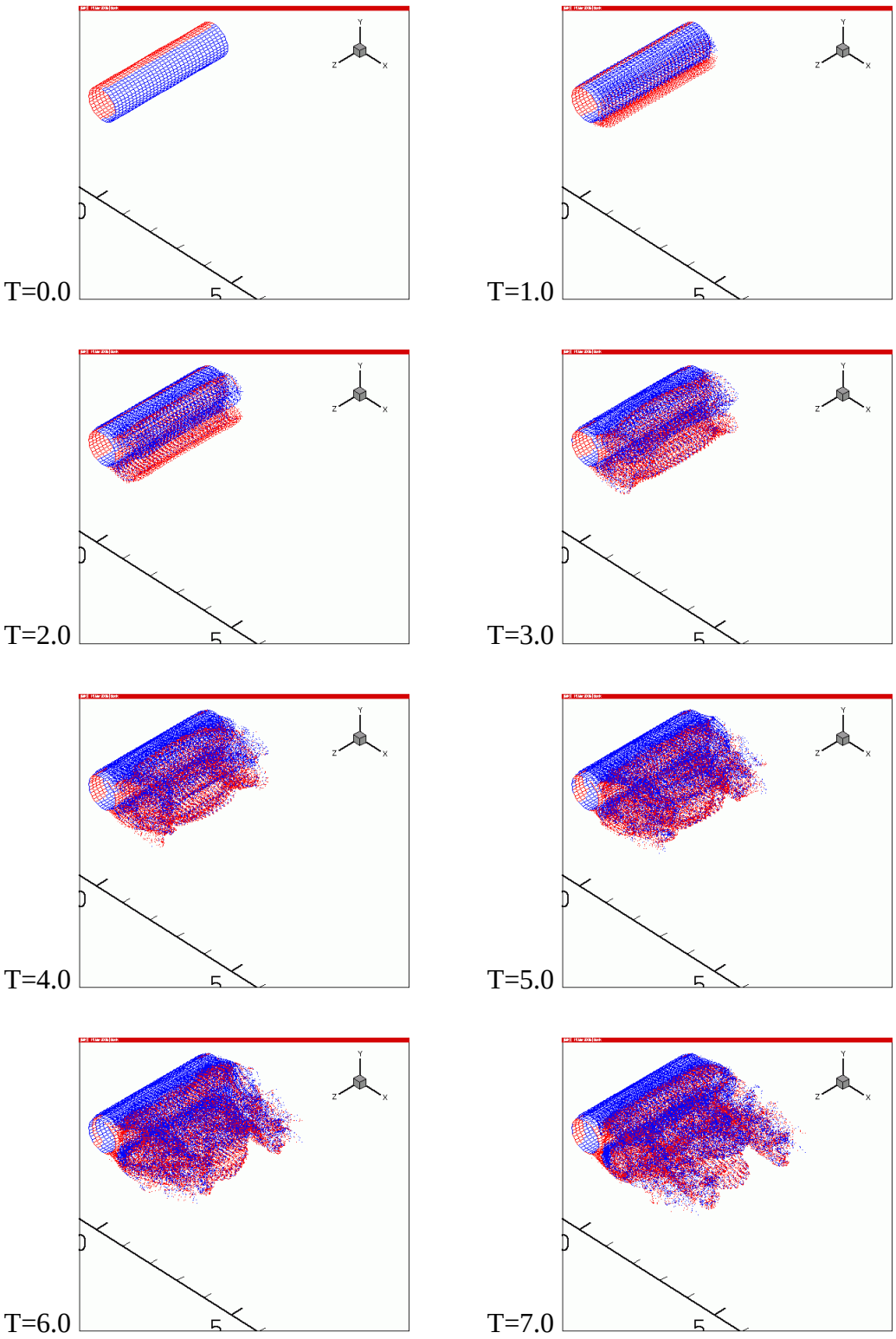


Figure 3.17: Perspective view of wake structures of circular cylinder from T=0.0 to T=7.0. Re=200

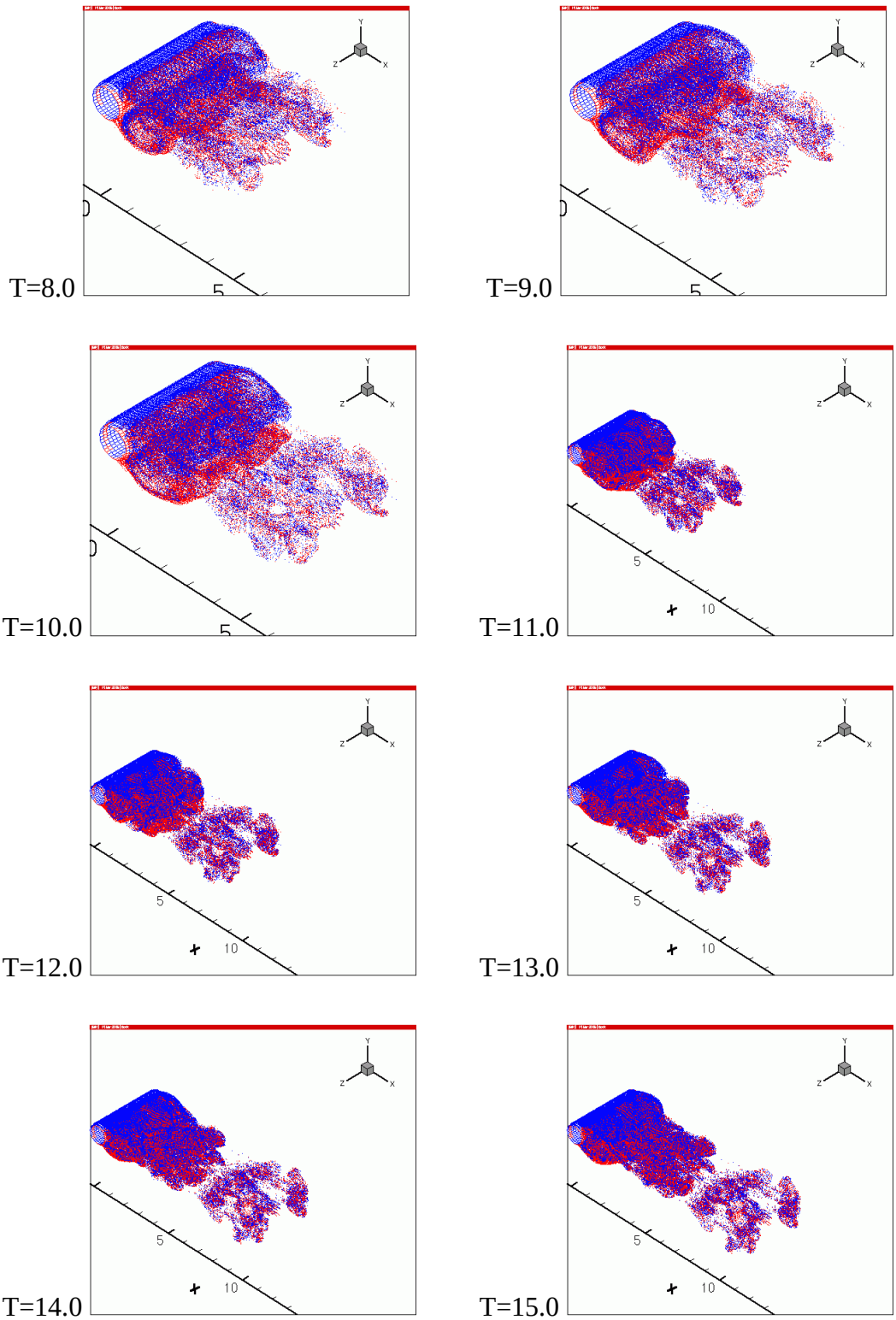


Figure 3.18: Perspective view of wake structures of circular cylinder from T=8.0 to T=15.0. Re=200

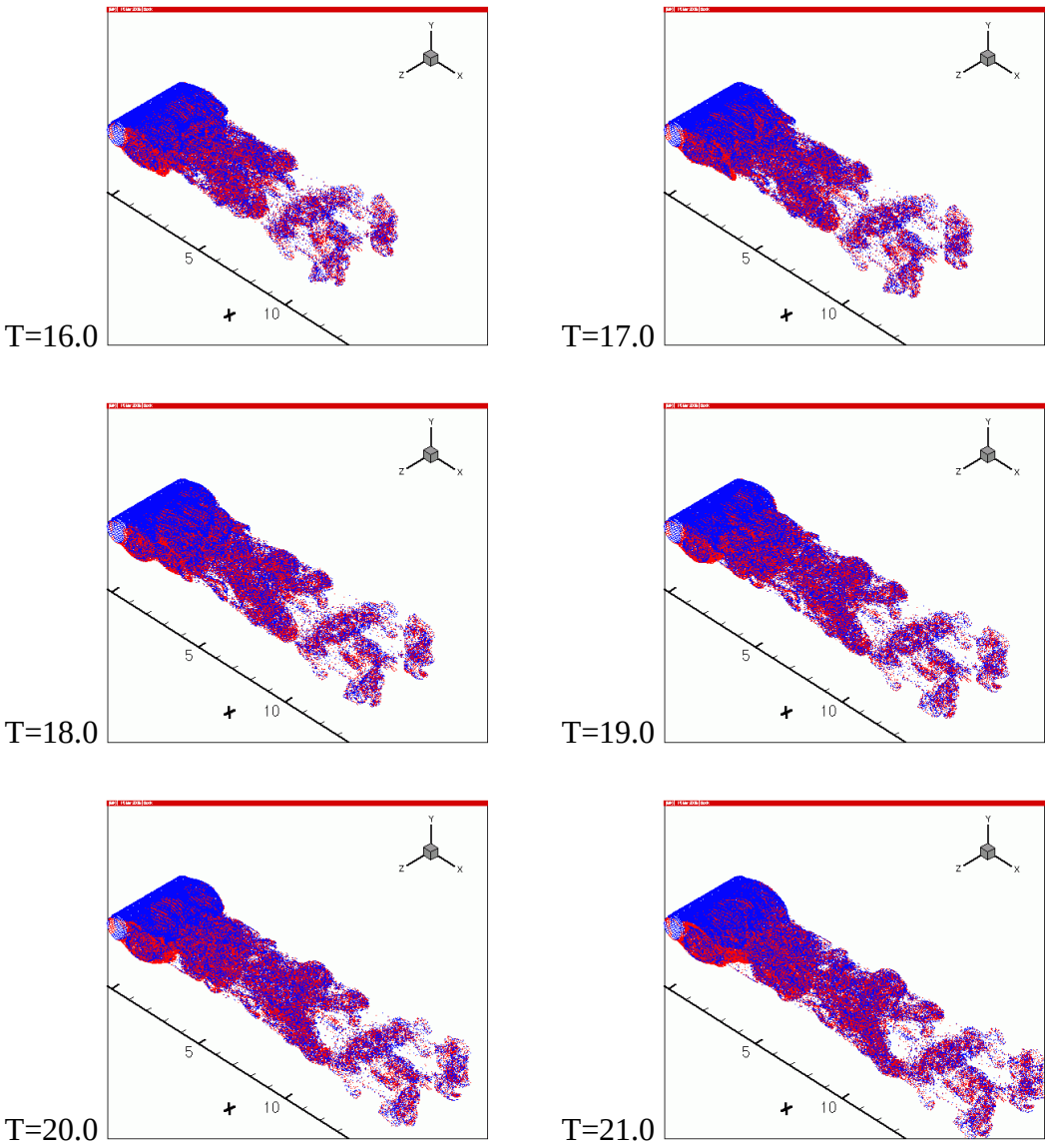


Figure 3.19: Perspective view of wake structures of circular cylinder from T=16.0 to T=21.0. Re=200

3.2.4 Case 3 (Simulation at Re=500)

3.2.4 Case 3 (Simulation at Re=500)

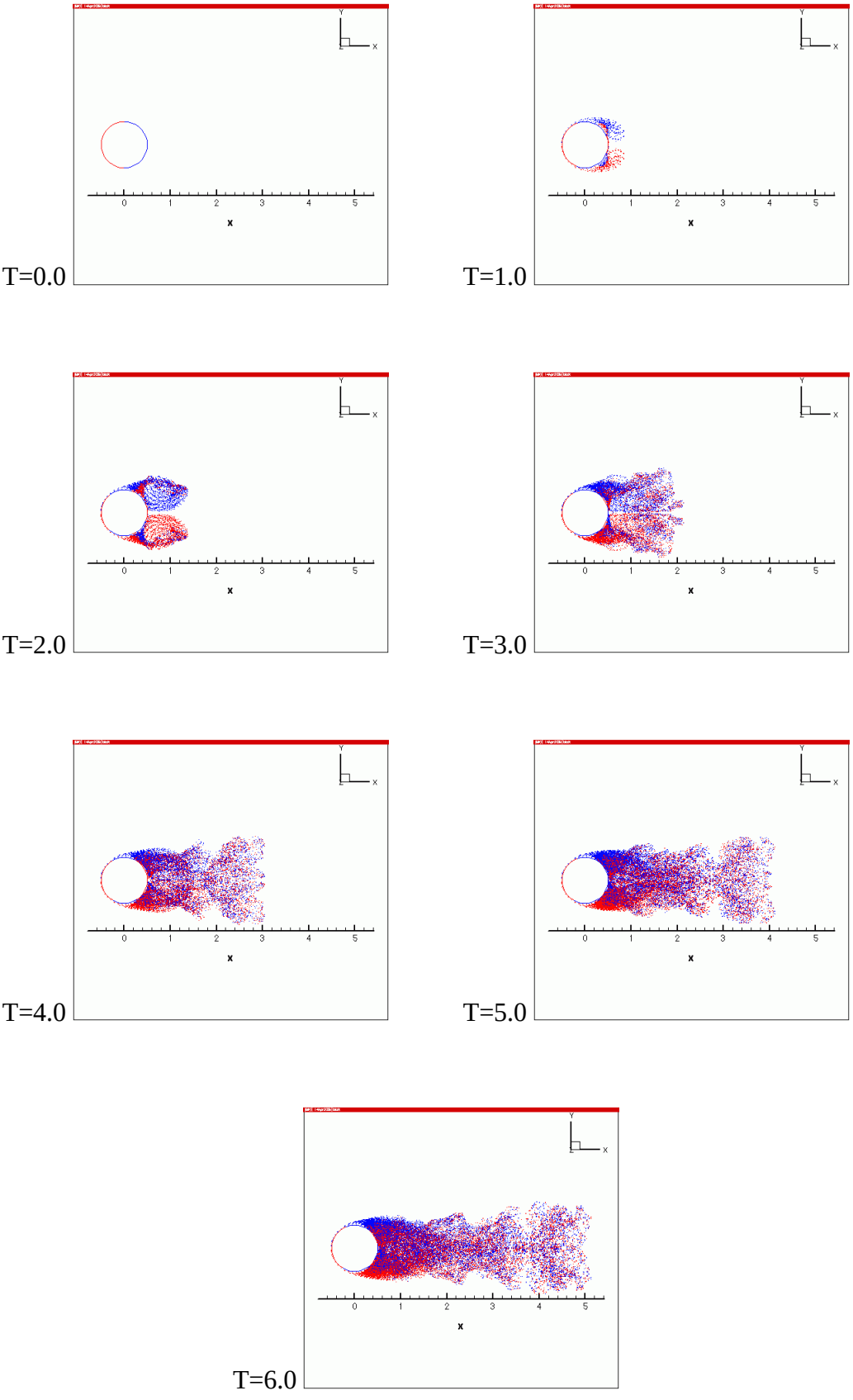


Figure 3.20: Wake structures of circular cylinder in XY plane, from T=0.0 to T=6.0. Re= 500

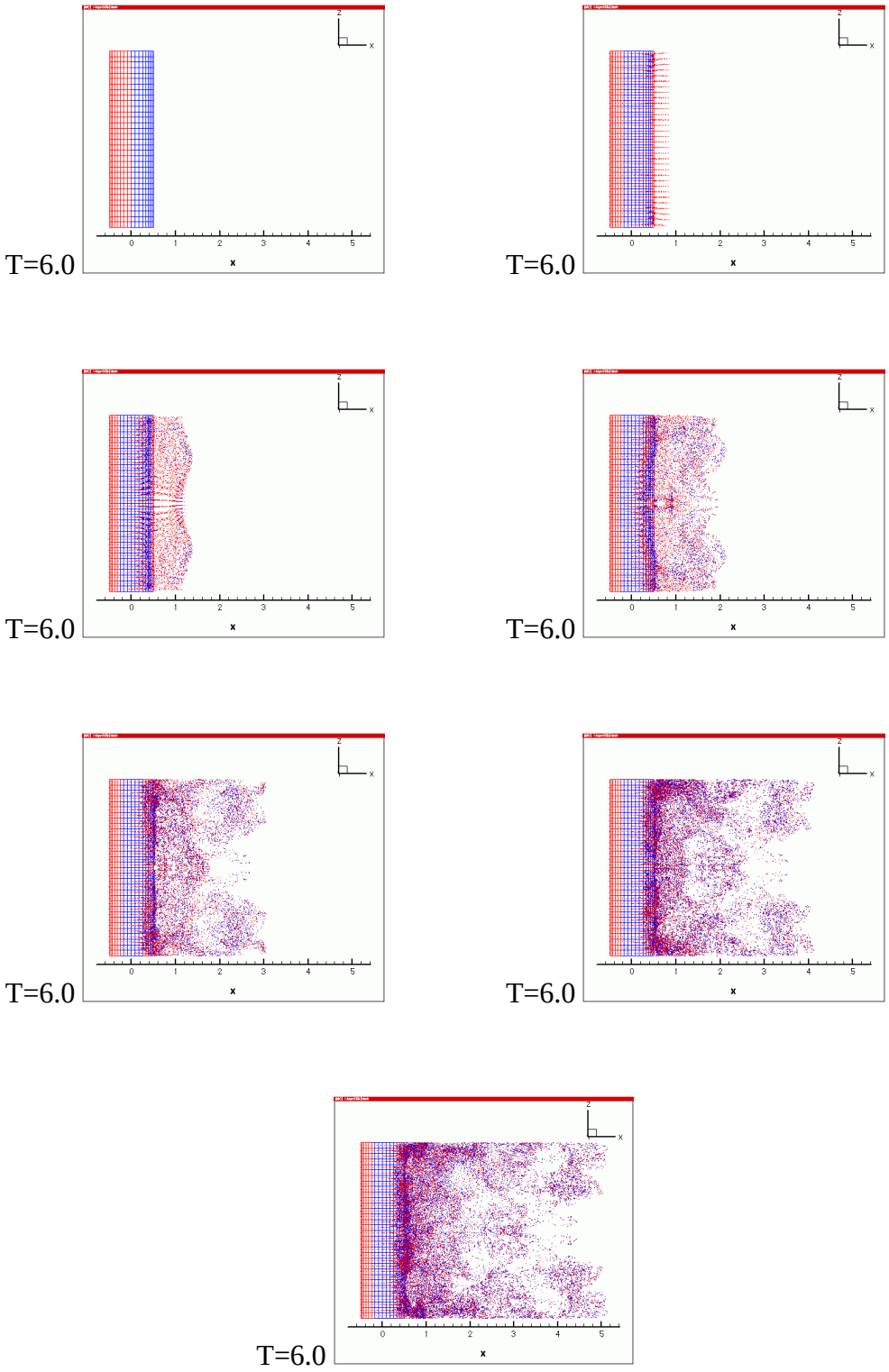


Figure 3.21: Wake structures of circular cylinder in XZ plane, from T=0.0 to T=6.0. Re=500

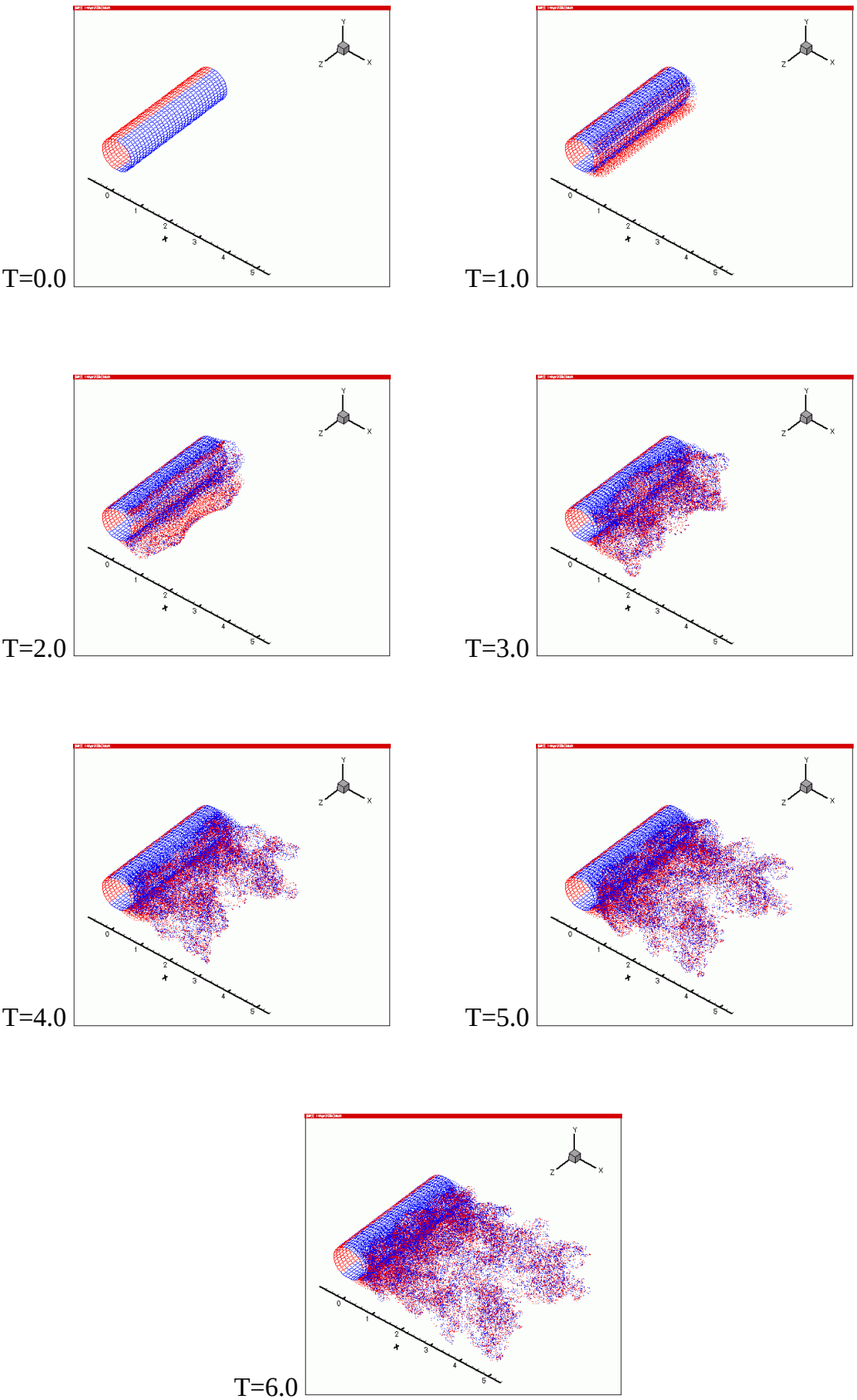


Figure 3.22: Perspective view of wake structure of circular cylinder from T=0.0 to T=6.0. R= 500.

3.3 Conclusion

In this study, three-dimensional separated viscous flows around a sphere and a circular cylinder have been calculated using a source and vortex panel method in combination with the Lagrangian discrete vortex method. Calculations have been performed at Re=50, 200 and 500.

The cylinder used in the investigation is represented with 1584 rectangular panels. For simulation of flow around a circular cylinder and its wake about 300.000 vortex elements are used. Parallel computing using MPI (Message Passing Interface) routines have been performed with a computer having 8x400 MHz IP35 processors and a memory size of 5120 MB. A typical computational time is on the order of a week.

The flow field and wake structure are compared by the previous works and good agreement has been found for the sphere. Then, the case of circular cylinder is studied. For the cylinder case, the image method is used in association with the panel method. So, as explained above, images of the cylinder with respect to the sidewalls are also included into the calculation.

For the cylinder case, flow field and wake structure are investigated at Reynolds numbers of 50, 200 and 500. At Re=50, side views of the separated flows indicate a much more originated wake structure as compared to those at Re=200 and 500 (Compare Figures 3.9, 3.12, 3.13, and 3.20). At Re=200, an instability is already developed around the outer edge of the large scale, symmetrically developing vortices behind the cylinder at the nondimensional time of 3. This instability resembles the thin share-layer instability (i.e. the Kelvin-Helmholtz instability as referred to in [40]). At Re=500, the symmetrically developed vortex wake is a diffused one as compared to those at Re=50 and 200 (Figures 3.9, 3.12, 3.20). It should be noted that, in obtaining the wake structures demonstrated herein, no artificial perturbation has been introduced in order to initiate a periodic shedding from upper and lower sides of the cylinder.

Therefore, symmetric wake behind the cylinder is obtained for large nondimensional times (Figure 3.14).

In summary, the simulation carried out herein is successful in predicting a widely known experimental finding indicating that the wake of the cylinder becomes more and more diffused as the Reynolds number increases.

Additionally, the top and the perspective views of the wake at Re=200 and 500 (Figures 3.15-3.19 and 3.21-3.22) indicate a spanwise waviness. It is known that [11] even at low Reynolds numbers, maintaining parallel vortex shedding to cylinder axis requires very carefully controlled end conditions. The numerical simulation herein is carried out for an infinitely long cylinder, and thus a parallel shedding is not expected for Re=200 and 500. However, a wavy wake is still present at a very low Reynolds number of 50 for even at low nondimensional times (Figure 3.10). This is in contrast to expectations and thought of as a result of unrealistic effect of sidewalls to the flow field as a whole. In a future study, more attention will be paid to the simulation of the flow field near the sidewalls as its effect may be amplified by the stretching terms in the vorticity transport equation and thus may result in an unexpected wavy wake at a rather low Reynolds numbers.

REFERENCES

[1] Sarpkaya, T., 1989. Computational Methods with Vortices – the 1988 Freeman Scholar Lecture, *Journal of Fluids Engineering, Trans. ASME,* **111**, 5-52.

[2] Kamemoto, K., 1995. On Attractive Features of the Vortex Methods, *Computational Fluid Dynamics Review*, Ed. M. Hafez and K. Oshima, John Wiley & Sons, 334-353.

[3] Leonard, A., 1980. Vortex Methods for Flow Simulations, *Journal of Computational Physics*, **37**, 289-335.

[4] Graham, J. M. R. 1988. Computation of Viscous Separated Flow Using a Particle Method, *Numerical Methods in Fluid Mechanics Vo. 3*, Oxford University Press

[5] Meneghini, J. R., Bearman, P. W., 1993. Numerical Simulation of High Amplitude Oscillatory Flow about a Circular Cylinder Using a Discrete Vortex Method, *AIAA Paper No 93-3288*,

[6] Shirayama, S., Kuwahara, K., Mendez, R., 1985. A New Three-Dimensional Vortex Method, *AIAA,* 85-1488.

[7] Greengard, C., 1985. The Core Spreading Vortex Method Approximates the Wrong Equation, *J. Comp. Phys.,* **61**, 345-348.

[8] Cheer, A. Y., 1989. Unsteady Separated Wake behind an Impulsively Started Cylinder in Slightly Viscous Fluid, *J. Fluid Mech.,* **201**, 485-505.

[9] Nakanishi, Y., Kamemoto, K., 1992. Numerical Simulation of Flow around a Sphere with Vortex Blobs, *Journal of Wind Engineering and Industrial Aerodynamics*, **46**, 363-369.

[10] Nakanishi, Y., Kamemoto, K. Mine, T., Noda, T., 1993. A Procedure to Estimate Unsteady Pressure Distributions for Vortex Method Using Boundary Element Method, *Proc. 5th Int. Symp. On Computational Fluid Dynamics, Sendai,* **2**, 313-318.

[11] Eisenlohr, H., Eckelmans, H., 1989. Vortex Splitting and its Consequences in the Vortex Street Wake of Cylinders at Low Reynolds Numbers, *Phys. Fluid,* A1,189-192.

[12] Keser, H. İ., Ünal, M. F., Bearman, P. W., 2001. Simulation of Wake form a Circular Cylinder with Spanwise Sinusoidal Waviness., *2.*

International Conference on Vortex Methods ITU Maçka Campus, Istanbul, Turkey, September 26-28, 131-137.

[13] Tombazis, N. Bearman, P. W., 1997. The Effects of Three-Dimensional Imposed Disturbances on the Bluff Body Near Wake Flows, *J. Fluid Mech.,* **330**, 85-112.

[14] Kamemoto, K., 2001. Engineering Application of the Vortex Methods Developed in Yokohama National University, *2. International Conference on Vortex Methods ITU Maçka Campus, Istanbul, Turkey, September 26-28,* 197-209.

[15] Nakanishi, Y., Kamemoto, K., 1994. Modification of Vortex Model for Consideration of Viscous Effect, *JSME International Journal Series B No 4* , **37**, 815-820.

[16] Winkelmans, G., Leonard, A., 1988. Improved Vortex Methods for Three-Dimensional Vortex Flows, *Proc. Workshop on Mathematical Aspects of Vortex Dynamics., Leeburg, Virginia,*25-35

[17] Schlichting, H., 1968, *Boundary Layer Theory, 6th Edition*, 82-84

[18] Kuwahara, K., 1978. Study of Flow Past a Circular Cylinder by an Inviscid Model, *J. Phys. Soc. Japan.,* **45**, 292-297.

[19] Lewis, R. I., 1981. Surface Vorticity Modeling of Separated Flows from Two-Dimensional Bluff Bodies of Arbitrary Shape, *Journal of Mechanical Engineering Science No.1,* **23**, 1-12.

[20] Chorin, A. J., 1978.Vortex Sheet Approximation of Boundary Layers, *J. Comp. Phys.,* **74**, 283-317.

[21] Cheer, A. Y., 1989.Unsteady Separated Wake behind an Impulsively Started Cylinder in Slightly Viscous Fluid, *J. Fluid Mech..,* **201**, 485-505.

[22] Kamemoto, K., 1994.Development of the Vortex Methods for Grid-Free Lagrangian Direct Numerical Simulation, *Proc. 3rd JSME-KSME Fluids Engineering Conference, Sendai,* 542-547.

[23] Kuwahara, K. Takami, H., 1973. Numerical Studies of Two-Dimensional Vortex Motion by a System of Point Vortices, *J. Fluid Mech.,* **57**, 247-253.

[24] Chorin, A. J., Bernard. P. S., 1973. Discretization of a Vortex Sheet with an Example of Roll-Up, *J. Comp. Phys..,* **13**, 423-429.

[25] Nakanishi, Y., Kamemoto, K., 1992. Numerical Simulation of Flow around a Sphere with Vortex Blobs, *Journal of Wind Engineering*, **52**, 267-272.

[26] Kamemoto, K., 2001. Engineering Application of The Vortex Methods Developed in Yokohama National University (YNU)., *2. International Conference on Vortex Methods ITU Maçka Campus, Istanbul, Turkey, September 26-28*, 197-209.

[27] Ojima A., Kamemoto, K., 1999. Numerical Simulation of Unsteady Flow around a Sphere by Vortex Method for Re Number from 300 to 1000, *1st International Conference on Vortex Methods, Kobe, Japan, November 4-5*, 83-91.

[28] Bearman P. W., 1998. Developments in the Understanding of Bluff Body Flows, *JSME International Journal- Series B*, **41**, No. 1, 103-114.

[29] Nakanishi, Y., Kamemoto, K., 2000. Numerical Simulation of Unsteady Flow around Three Dimensional Bluff Bodies by an Advanced Vortex Method, *JSME International Journal Series B No2*, **43**, 127-135.

[30] Ünal, M. F., Kamemoto, K., 1999. Simulation of Three Dimensional Separated Flow around an Ellipsoid by Discrete Vortex Method. *First International Conference on Vortex Methods, Kobe, Japan, November 4-5, 107-112*.

[31] Nakanishi, Y., Kamemoto, K., Nishio, M., 1994. Modification of Vortex Model for Consideration of Viscous Effect (Examination of Vortex Model Interaction of Vortex Rings), *JSME International Journal Series B No 4*, **37**, 815-820.

[32] Lee, S. H., Jin, D. S., Yoon, J. S., 2002. Comparisons of Two Viscous Models for Vortex Methods in Parallel Computation, *JSME International Journal Series B No 2*, **45**, 231-239.

[33] Koç, S., May 2002, Vortex-Induced Vibrations of an Elastically Mounted Circular Cylinder in Two Degrees of Freedom, *M.Sc. Thesis Istanbul Technical University Institute of Science and Technology*.

[34] Çete, A. R., February 1995, Simulation of Separated Flow around Cylinders, *M.Sc. Thesis Istanbul Technical University Institute of Science and Technology*.

[35] Anderson, J. D. , 1985. Fundamentals of Aerodynamics, *McGraw-Hill Book Company, Singapore*.

[36] Currie, I. G. , 1993. Fundamental Mechanics of Fluids, *McGraw-Hill Book Company, Singapore*.

[37] Milewski, E. G., 1984. The Vector Analysis Problem Solver / Staff of Research and Education Association, *Research & Education Association, New York*.

[38] Pachoce, P. S., Ming, W. C. 1997. Introduction to Message Passing Programming MPI User Guide in Fortran, *Computer Centre, University of Hong Kong, Hong Kong*.

[39] Cheer, A. Y., 1989. Unsteady Separated Wake behind an Impulsively Started Cylinder in Slightly Viscous Fluid, *J. Fluid Mech.,* **201**, 485-505.

[40] Unal, M. F., Rockwell D. 1988. On Vortex Formation from a Cylinder. 1. The Initial Instability, *J. Fluid Mech.,* **190**, 491-512.

[41] http://artemis.cc.itu.edu.tr/ebt-bin/nph-dweb/dynaweb

[42] http://www.nas.nasa.gov/Groups/SciCon/Tutorials/MPIintro/toc.html

[43] http://www-unix.mcs.anl.gov/mpi/index.html

[44] http://www.mpi-forum.org/

[45] http://www-unix.mcs.anl.gov/mpi/www/

APPENDIX A1

COMPLEX IDENTITIES INVOLVING CURL, DIVERGENCE AND GRADIENT OPERATORS

Identity 1:

$$(\mathbf{a}\cdot\nabla)\cdot\mathbf{a}=\frac{1}{2}\nabla a^2-\mathbf{a}\times(\nabla\times\mathbf{a}) \tag{A1.1}$$

Proof: The left-hand side of equation (A1.1) represents a vector, the right-hand side is also a vector. It is sufficient to perform the calculations for the first component and show that the first component of the vector on the left-hand side of the equation is equal to the right-hand side of the equation. The other components can be obtained from symmetry.

The first component of the left-hand side vector is equal to:

$$[(\mathbf{a}\cdot\nabla)\mathbf{a}]_1=(a_1\frac{\partial}{\partial x}+a_2\frac{\partial}{\partial x}+a_3\frac{\partial}{\partial x})a_1=a_1\frac{\partial a_1}{\partial x}+a_2\frac{\partial a_1}{\partial x}+a_3\frac{\partial a_1}{\partial x} \tag{A1.2}$$

Here $[...]_1$ indicates the first component of the vector in the bracket.

The first component of the right-hand side vector is equal to:

$$\begin{aligned}&[(\mathbf{a}\cdot\nabla)\cdot\mathbf{a}=\frac{1}{2}\nabla a^2-\mathbf{a}\times(\nabla\times\mathbf{a})]_1\\&=\frac{1}{2}\frac{\partial}{\partial x}(a^2)-[\mathbf{a}\times(\nabla\times\mathbf{a})]_1\\&=\frac{1}{2}\frac{\partial}{\partial x}({a_1}^2+{a_2}^2+{a_3}^2)-(a_2[\nabla\times\mathbf{a})]_3-a_3[\nabla\times\mathbf{a})]_2)\\&=\frac{1}{2}\frac{\partial}{\partial x}({a_1}^2+{a_2}^2+{a_3}^2)-[a_2(\frac{\partial a_2}{\partial x}-\frac{\partial a_1}{\partial y})-a_3(\frac{\partial a_1}{\partial z}-\frac{\partial a_3}{\partial y})]\end{aligned} \tag{A1.3}$$

$$\begin{aligned}&=a_1\frac{\partial a_1}{\partial x}+a_2\frac{\partial a_2}{\partial x}+a_3\frac{\partial a_3}{\partial x}-a_2\frac{\partial a_2}{\partial x}+a_2\frac{\partial a_1}{\partial y}+a_3\frac{\partial a_1}{\partial z}-a_3\frac{\partial a_3}{\partial x}\\&=a_1\frac{\partial a_1}{\partial x}+a_2\frac{\partial a_1}{\partial y}+a_3\frac{\partial a_1}{\partial z}\end{aligned}$$

Form equation (A1.2) and (A1.3), we conclude that the first components are equal. It follows immediately that the second and third components are also equal.

Identity 2:

$$curl(\mathbf{a}\times\mathbf{b}) = \mathbf{a}div\mathbf{b} - \mathbf{b}div\mathbf{a} + (\mathbf{b}\cdot\nabla)\mathbf{a} - (\mathbf{a}\cdot\nabla)\mathbf{b} \tag{A1.4}$$

Proof: Here, again it will be proved that the first component of the vector on the left-hand side of the equation (A1.4) is equal to the right-hand side of the equation. By symmetry, all the calculations can be rewritten for the second and third component. We have

$$\begin{aligned}[curl(\mathbf{a}\times\mathbf{b})]_1 &= \frac{\partial}{\partial y}[\mathbf{a}\times\mathbf{b}]_3 - \frac{\partial}{\partial z}[\mathbf{a}\times\mathbf{b}]_2 \\ &= \frac{\partial}{\partial y}(a_1b_2 - a_2b_1) - \frac{\partial}{\partial z}(a_3b_1 - a_1b_3)\end{aligned} \tag{A1.5}$$

The firts component of the vector on the right-hand side of equation (A1.4) is equal to:

$$\begin{aligned}&[\mathbf{a}div\mathbf{b} - \mathbf{b}div\mathbf{a} + (\mathbf{b}\cdot\nabla)\mathbf{a} - (\mathbf{a}\cdot\nabla)\mathbf{b}]_1 \\ &= a_1 div\mathbf{b} - b_1 div\mathbf{a} + (\mathbf{b}\cdot\nabla)a_1 - (\mathbf{a}\cdot\nabla)b_1 \\ &= a_1(\frac{\partial b_1}{\partial x} + \frac{\partial b_2}{\partial y} + \frac{\partial b_3}{\partial z}) - b_1(\frac{\partial a_1}{\partial x} + \frac{\partial a_2}{\partial y} + \frac{\partial a_3}{\partial z}) \\ &+(b_1\frac{\partial}{\partial x} + b_2\frac{\partial}{\partial y} + b_3\frac{\partial}{\partial z})a_1 - (a_1\frac{\partial}{\partial x} + a_2\frac{\partial}{\partial y} + a_3\frac{\partial}{\partial z})b_1 \\ &= a_1\frac{\partial b_1}{\partial x} + a_1\frac{\partial b_2}{\partial y} + a_1\frac{\partial b_3}{\partial z} - b_1\frac{\partial a_1}{\partial x} - b_1\frac{\partial a_2}{\partial y} - b_1\frac{\partial a_3}{\partial z} \\ &+b_1\frac{\partial a_1}{\partial x} + b_2\frac{\partial a_1}{\partial y} + b_3\frac{\partial a_1}{\partial z} - a_1\frac{\partial b_1}{\partial x} - a_2\frac{\partial b_1}{\partial y} - a_3\frac{\partial b_1}{\partial z} \\ &= \frac{\partial}{\partial y}(a_1b_2) - \frac{\partial}{\partial y}(a_2b_1) + \frac{\partial}{\partial z}(a_1b_3) - \frac{\partial}{\partial z}(b_1a_3) \\ &= \frac{\partial}{\partial y}(a_1b_2 - a_2b_1) + \frac{\partial}{\partial z}(a_1b_3 - b_1a_3)\end{aligned}$$

Thus, the first components are equal. In the same manner, it can be shown that the second and third components are also equal.

BIOGRAPHY

Kürşat KARA was born in Kozan, Adana in 1978. He graduated from the Kozan High School in 1995. At the same year he enrolled I.T.U., Department of Aeronautical Engineering. He obtained his B.Sc. degree in 1999 and then started his graduate education in I.T.U., Institute of Science and Technology, Aeronautical Engineering Department. He has been working in Faculty of Aeronautics and Astronautics at I.T.U. as a research assistant since 2000.